Biochemical Characterization of a New Subfamily of Unusual Pathogenic Fungal Lipoxygenases

By

S. Gage Hill

Date: July 2024

Director of Thesis: Adam R. Offenbacher

Major Department: Chemistry

ABSTRACT

Lipoxygenases (LOX) are a family of enzymes that catalyze the (per)oxidation of polyunsaturated fatty acids. Over the last 30 years, fungal lipoxygenases have drawn interest because of their potential role in plant pathogenesis. This family of LOXs is distinct from the canonical LOXs in plants and animals due to i) nature of their metal center, ii) formation of a unique bis-allylic product, iii) post-translation, N-linked glycosylation, and iv) secreted from their host organism and implicated in pathogenesis. To date, six fungal LOXs have been biochemically characterized. A recent bioinformatics study revealed a potential new subfamily of fungal lipoxygenases, which deviate from the six 'prototype' fungal LOXs. These so-called 'class II' fungal LOXs have a cysteine amino acid where an otherwise conserved leucine residue is found across all LOXs. The Leu is considered a "substrate clamp" and previous mutations of this residue to volume-reducing alanine are linked to impairment of enzyme activity. Currently, there is no biochemical data reported for these putative class II fungal LOX enzymes. Herein, we use a combination of biochemical characterization methods and protein modeling to analyze

three representative class II LOXs. The enzymes were successfully isolated from yeast expression cultures but showed no enzyme activity. AI generated structural models coupled with circular dichroism spectroscopy suggest that these enzymes fold similarly to that of LOXs, including nearly identical primary coordination sphere residues. Metal analysis indicates that the proteins can accommodate manganese or iron, consistent with other LOXs. To understand the functional consequence of these non-conserved mutations, a Leu-to-Cys variant was prepared for a paradigm plant LOX from soybean seeds. This variant is catalytically impaired. The collective data indicates that the class II LOXs are not effective at LOX activity; their potential biochemical function is discussed.

Biochemical Characterization of a New Subfamily of Unusual Pathogenic Fungal Lipoxygenases

A Thesis

Presented to the Faculty of the Department of Chemistry

East Carolina University

In Partial Fulfillment of the Requirements for the Degree

Master of Science in Chemistry

By

S. Gage Hill

July 2024

Director of Thesis: *Dr. Adam R. Offenbacher, Ph.D.*

Thesis Committee Members:

Morgan Milton, Ph.D.

Dr. Colin Burns, Ph.D.

ACKNOWLEDGEMENTS

I cannot begin to express my gratitude to Dr. Offenbacher, who recruited me to conduct research as an undergraduate from a general chemistry lab in the spring of 2020. I wasn't sure how strongly I was interested in research, and my career goals weren't clear. He has been the best mentor I could ask for in terms of both future career success and my maturity, and for that, I'm deeply grateful. Dr. Offenbacher's passion for science has been a constant source of inspiration and motivation in both my research and in life. His impact will forever be treasured.

Additionally, I would like to thank the Offy lab group students during my 3+ years in the lab. I cherish my friendships and have learned so much from each of you. Starting from my undergraduate days with Ethan Patel and our continuous collaboration, and up until now with valuable advice and support from current lab mates, Andrew and Wyatt.

Lastly, I would like to thank my family and my friends, who have made ECU so special. My parents have always been supportive of my choices and ambitions, and I'm forever grateful for that. To my friends, my love for ECU would not be as strong without you, for you've been a constant source of support and entertainment.

TABLE OF CONTENTS

LIST OF TABLES

LIST OF FIGURES

Chapter One

Introduction

1.1 Introduction to Lipoxygenases: Function

Lipoxygenases (LOXs) are a family of enzymes that oxidize polyunsaturated fatty acids and create bioactive cell-signaling mediators found widely in plants, animals, fungi, and some prokaryotes.[1–3] Plant and animal LOXs are the most thoroughly characterized and considered canonical enzymes of the family, though they have different biological functions and substrate preferences. In plants, a common product that functions in the stress response of plants is jasmonic acid, which is a downstream product from linolenic acid oxidation by the LOX pathway.[1,4] Mammalian LOXs produce anti-inflammatory lipoxins or pro-inflammatory lipid mediators such as leukotrienes.[2] The latter are produced when the body encounters an allergen, thus activating an immune response.[5]

Plant and animal LOXs use a non-heme, mononuclear ferric hydroxide cofactor to oxidize fatty acids and generate a conjugated, hydroperoxide (HpOD) product.[6] Plant LOXs prefer the oxidation of shorter chain fatty acids, such as linoleic acid (LA; C18:2), whereas animals prefer longer chain fatty acids, such as arachidonic acid (AA; C20:4). This reaction is initiated by hydrogen abstraction at the bis-allylic carbon-hydrogen bond (at carbon *n*) of the substrate through a proton coupled electron transfer (PCET) process (**Figure 1.1**), generating a delocalized substrate-centered organic radical. Oxygen insertion usually takes place at *n + 2* or *n – 2* carbon, producing a cis-trans-conjugated hydroperoxyl fatty acid **(Figure 1.1**).[7] The classical

LOXs are named based on where oxygen is inserted into the fatty acid; for example, plant LOXs make 9*S*/*R*- and 13*S*/*R*-HpOD products from LA.

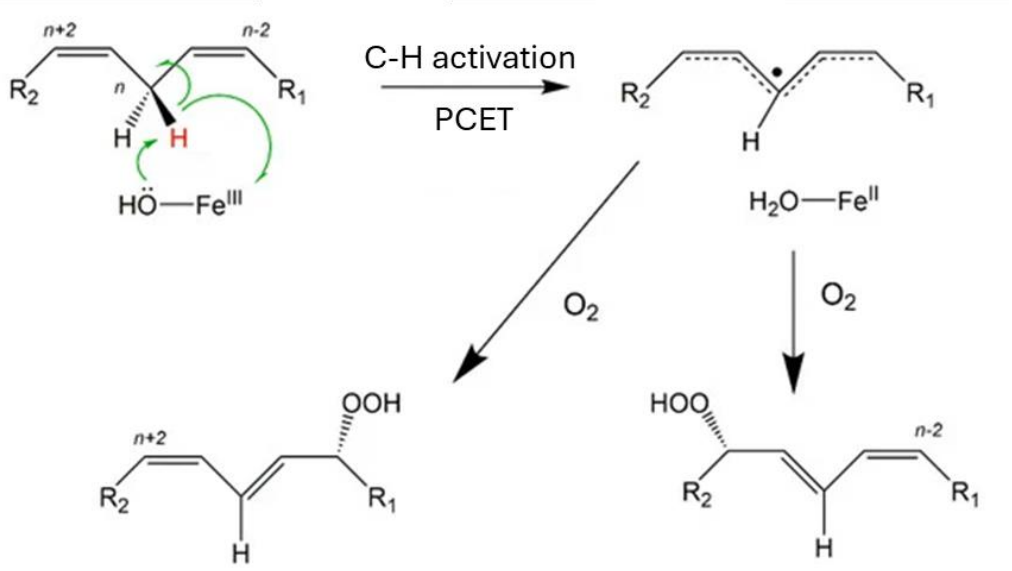

Figure 1.1: *Representative LOX reaction mechanism, with the oxidation of substrate LA by model lipoxygenases. The C-H cleavage occurs via PCET. The C-H cleavage step is rate-determining, based on the large kinetic isotope effects (KIE).*[2]

1.2 Kinetic isotope effects and hydrogen tunneling

Kinetic isotope effects (KIEs) are the ratio of reaction rates between an atom of a light isotope and a heavy isotope. One example is the primary deuterium KIEs, which is ratio of rate of hydrogen transfer versus rate of deuterium transfer (i.e., $^{D}KIE = k_H/k_D$). This method is often used in biochemistry to obtain information on the rate-determining step of an enzyme reaction. The classical limits of KIEs, set by the Bell correction models, are based on the difference in the thermal energy of the ground state stretching vibration of the bond being broken. For a C-H vs C-D bond cleavage reaction, the upper limit of the ^{D}KIE is theorized to be ~7 for classical

transition state theory.[8] For the LOX reaction, several ^{D}KIE studies have been reported for the oxidation of fatty acids, with the primary ^{D}KIE of the first-order rate constant (i.e., k_{cat}) ranging from 20 to nearly 100.[9] These large isotope effect values are indicative of the C-H cleavage step being the rate-limiting step. Furthermore, the large magnitude of ^{D}KIE is consistent with the hydrogen transfer occurring via a tunneling mechanism.[10] Tunneling is a quantum phenomenon that suggests proton (or hydrogen atom) transfer 'tunnels' through the energy barrier instead of over-the-barrier crossing (**Figure 1.2**). The magnitude of the activation energy (E_a) of these tunneling reactions may reflect the protein structural sampling to achieve degenerate wavefunction overlap for effective hydrogen transfer.[10]

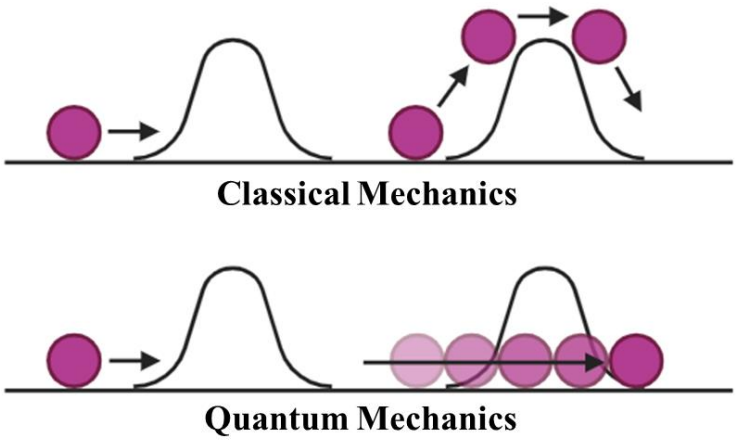

***Figure 1.2**: Classical mechanics where the proton transfer requires energy to pass over the barrier, and quantum mechanics involving the transfer through the energy barrier instead of over.*

1.3 General LOX structure

The global protein structures of plant and animal LOXs contain a large catalytic domain that is predominantly α-helical and approximately 500-700 amino acids in length (**Figure**

1.3A,B; green); plant LOXs are ~150 amino acids larger in comparison to animal LOXs, with the difference in length from additional loop extensions at the surface.[11] Within the catalytic domain, there is a U-shaped hydrophobic substrate binding channel, which differs in size based on the preferred substrate. The mononuclear, non-heme iron center is coordinated in a distorted octahedral geometry by the carboxyl group of the C-terminal tail, the side chain of 3 histidine, an asparagine, and a water molecule (**Figure 1.3C**).[12]

Secondly, these LOXs contain a PLAT (Polycystin-1, Lipoxygenase, Alpha-Toxin) domain which is suggested to be involved in membrane association; this domain is arranged as a β-barrel structure (**Figure 1.3A,B;** wheat).[13] Removal or mutation of this accessory domain often leads to structural instability of the catalytic domain, variations in catalytic rates, and affected substrate specificity.[2]

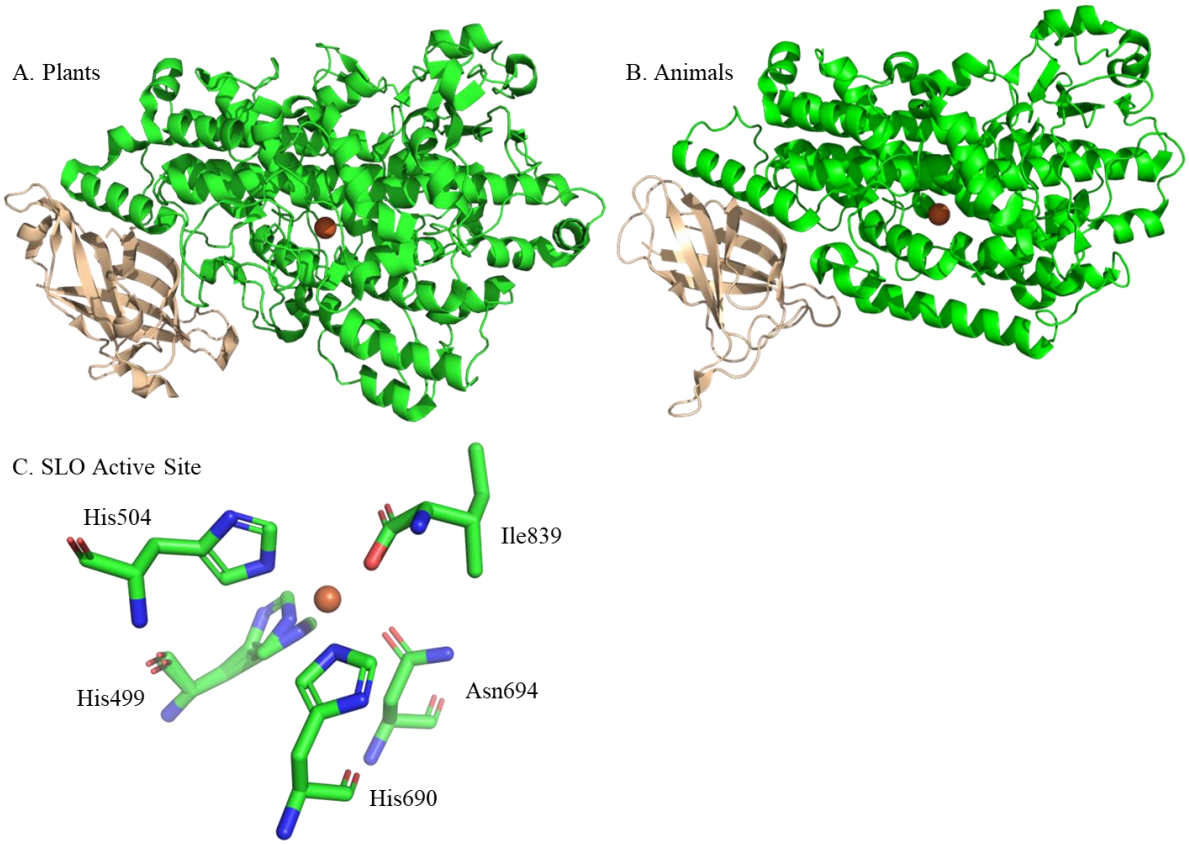

***Figure 1.3**: General enzyme structures for the representative lipoxygenases from (A) plants and (B) animals. The catalytic domain is represented in green, while the PLAT domain is represented in wheat. (C) The active site of SLO is ligated by five amino acids and a water (not shown).[12] (A) PDB: 3PZW, (B) PDB: 4NRE*

1.4 Emergence of 'non-canonical' fungal LOXs

Fungal LOXs were first discovered and isolated around 30 years ago.[14] The first one to be discovered was from the take-all wheat fungus, *Gaeumannomyces graminis*.[15] Initial biochemical experiments focused on the protein isolated from the fungus, with yields of 0.45 mg/L of the protein isolated from the host organism. Since then, four other fungal LOXs have been isolated from recombinant expressions using either yeast (*P. pastoris*) or bacteria (*E. coli*).[16–18]

From the emerging biochemical studies on such fungal LOXs, this family has exhibited distinct differences from the canonical LOXs in plants and animals.[19] To summarize, the fungal

LOXs i) are decorated with post-translational, *N*-linked glycans at the protein surface, ii) often contain a manganese catalytic center rather than a mononuclear iron center, iii) lack the N-terminal PLAT domain found in plants and animal LOXs (**Figure 1.4**), and iv) generate a unique bis-allylic 11S-HpODE product from the oxidation of LA.

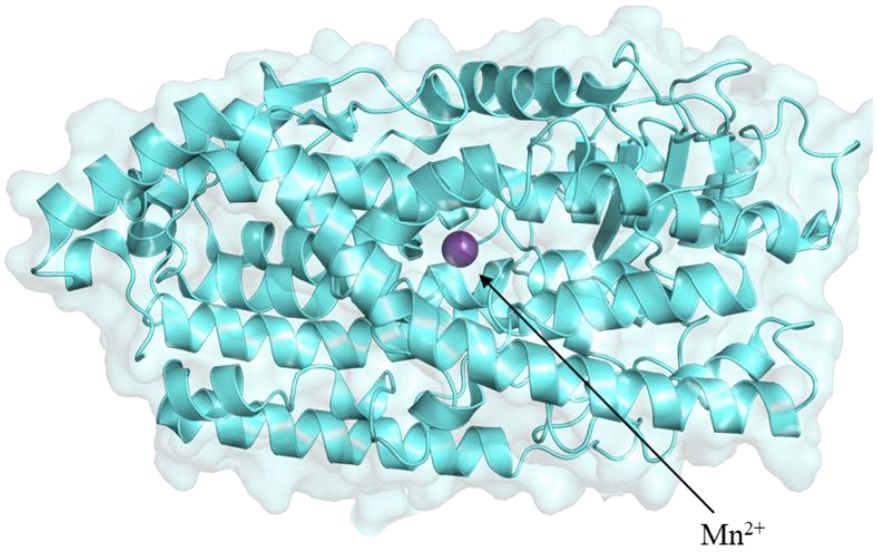

Figure 1.4: *Crystal structure of the LOX from Magnaporthe oryzae (Mo). PDB: 5FNO*[7]

Of the six characterized manganese lipoxygenases (Mn-LOX), five of those originate from plant-pathogenic fungi.[20] Those five LOXs derive from *M. oryzae* (*Mo*) *M. salvinii*, *F. oxysporum*, *C. gloeosporioides*, and *G. graminis* (*Gg*).[3,14,18,21] The top plant-pathogenic fungi in molecular plant pathology is *Magnaporthe oryzae*, or the rice blast fungus. This pathogenic fungus affects a third of the world's rice crops annually, which would feed approximately 60 million people. This has a substantial global impact, it is estimated that half of the world's population uses rice as its primary source of caloric intake.[22] Thus, this fungus has a devastating

impact on the world's food source. Instead of the PLAT domain, these fungal LOX genes contain an encoded N-terminus secretory signal sequence that promotes secretion of the enzymes, often along with other enzymes during pathogenesis.[20] For example, analysis of mRNA levels of *Mo*LOX biosynthesis revealed that the enzyme is formed and secreted during at its peak during the formation of the appressorium, the fungal body, marking the onset of pathogenesis.[16] Thus, these secreted LOXs are expected to play an important role in the plant pathogenesis.

1.5 N-linked Glycosylation

Glycosylation is a post-translational modification (PTM) used to attach carbohydrates (glycans) on the surface of the protein. Glycans serve multiple functions, such as protein folding, protein trafficking, membrane presentation, stabilization, and in the protective effort against proteolysis.[8] Glycosylation of manganese lipoxygenases was first discovered in 1998 in *Gg*LOX when the enzyme was purified from its host organism.[14] From recombinant expressions, *Mo*LOX is isolated with seven to eight *N*-linked glycans.[23] *N*-linked glycans are appended to an asparagine with the sequon Asn-X-Thr/Ser, where X is not Pro or Asp. A way to test for glycosylation from a protein sample is using sodium dodecyl sulfate polyacrylamide gel electrophoresis (SDS-PAGE). SDS-PAGE analysis of *Gg*LOX and *Mo*LOX samples show bands that smear and migrate with masses in excess of 100 kDa.[24] The corresponding theoretical masses of the proteins are 65-70 kDa.[15,16] Thus, the SDS-PAGE data are consistent with the attachment of several heterogenous, *N*-linked glycans. Glycans prevent crystal packing when attempting to obtain a crystal structure of the enzyme, so the purified enzymes were de-

glycosylated using α-mannosidase and endoglycosidase H to promote crystallization and structure determination (**Figure 1.5A**).[7,23]

Enzyme kinetic studies reveal essential information on enzymes such as substrate specificity, pH preference and dependence, temperature dependence, rate of catalysis, and more. The k_{cat} of *Mo*LOX is unchanged over a pH range of 7-9, indicating that the enzyme is pH independent.[23] Kinetic studies often use pH 9.0 when analyzing *Mo*LOX, as the critical micelle concentration of fatty acid substrates are pH dependent and are elevated at higher pH values. The reaction with LA is also associated with a large, temperature independent kinetic isotope effects, supporting that the hydrogen transfer from C-H cleavage is rate-limiting and occurs by tunneling in fungal LOXs.[23]

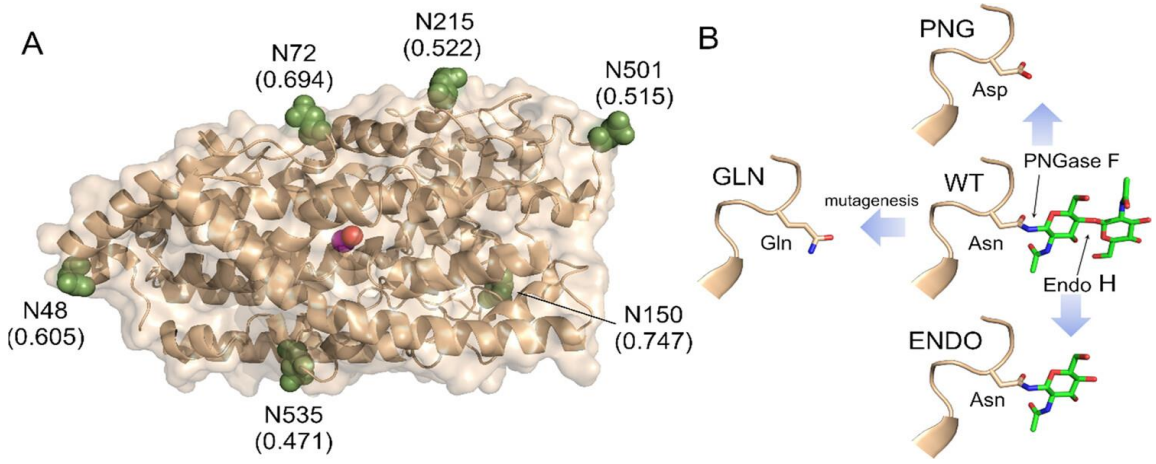

Figure 1.5: *X-ray crystal structure of MoLOX with the Asn residues forming putative N-linked glycosylation sites shown as spheres (A). The potential for N-linked glycosylation sites is listed in parentheses. The catalytic cofactor, Mn^{2+}–OH_2, is represented as purple and red spheres, respectively. (B) Diagram illustrating the methods for N-linked glycan processing (blue arrows). The green sticks represent N-acetylglucosamine (N-GlcNAc) residues, and the full glycan structures have been removed for clarity. For "GLN" MoLOX variant, all eight asparagine residues that are predicted N-linked glycosylation sites were mutated to glutamine.*[8]

Recent *Mo*LOX studies have removed glycans in a handful of ways to gather information on effects on structure and potential function in catalysis. The glycans were removed from the enzyme using PNGaseF, endoglycosidase H (EndoH), and Asn-to-Gly mutagenesis (**Figure 1.5B**).[8,25] Studies included proteolytic stability, kinetics, and structural tests. SDS-PAGE analysis of the *Mo*LOX treatments to remove (or alter) glycans showed increased susceptibility of the proteins to degradation by trypsin in limited proteolysis experiments (**Figure 1.6**). Most notably, the Asn-to-Gln mutated enzyme (**Figure 1.5B**) without glycosylation sites was most susceptible to trypsin. Since these enzymes are secreted by their natural hosts, these limited proteolysis data indicate that the glycans provide stability against proteolytic degradation.[8] The removal of the glycans from the enzyme results in only minor changes of kinetic activity, though local changes in the protein dynamics may account for the differences in substrate selectivity.

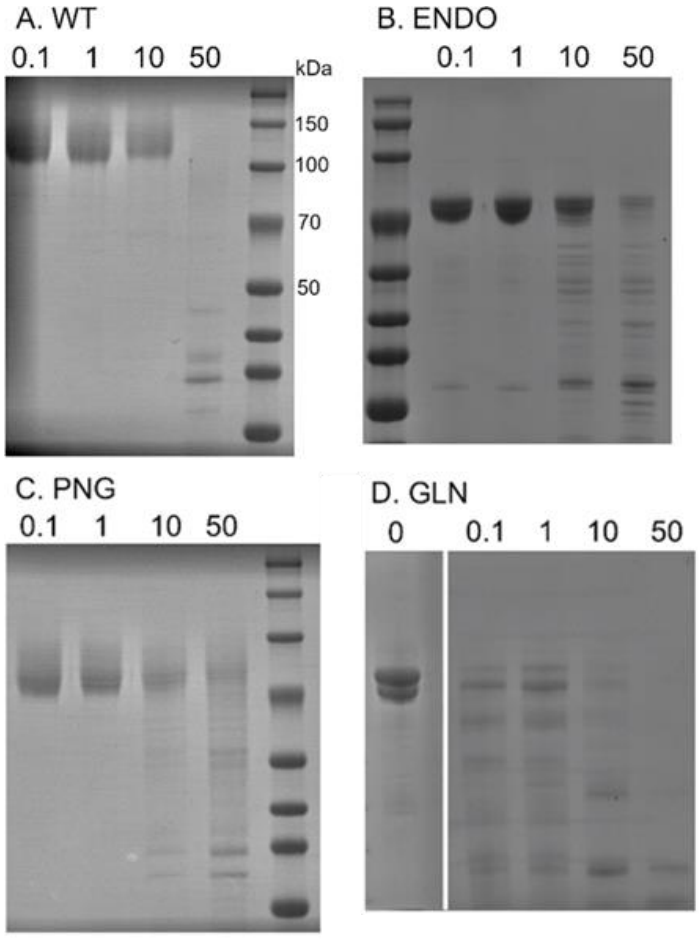

Figure 1.6: *SDS-PAGE analysis of (A.) WT MoLOX, (B.) MoLOX treated with EndoH, and (C.) MoLOX treated with PNGase, and (D.) Asn-to-Gly MoLOX variant in the presence of trypsin (0.1-50 µL).*[8]

1.6 Manganese as a catalytic cofactor

Fungal LOXs contain a manganese catalytic center, whereas plant and animal LOXs contain an iron cofactor.[26] Substitution of iron for manganese in the model plant lipoxygenase from soybean (SLO), led to an inactive enzyme.[27] A crystal structure of the Mn-substituted SLO (**Figure 1.7**) was nearly superimposable to that of the native Fe^{2+} form.[27] Crystal structures of *Gg*LOX and *Mo*LOX show similar ligands to the Mn^{2+} as Fe^{2+} center in plant and animal orthologues (**Figure 1.7**).[7,28] Further, the second-shell hydrogen-bonding network is distinct

between iron and fungal LOXs. The differences in the orientations of the primary ligand environment, which may be influenced by the second-shell ligands, might be responsible for the different reactivities.

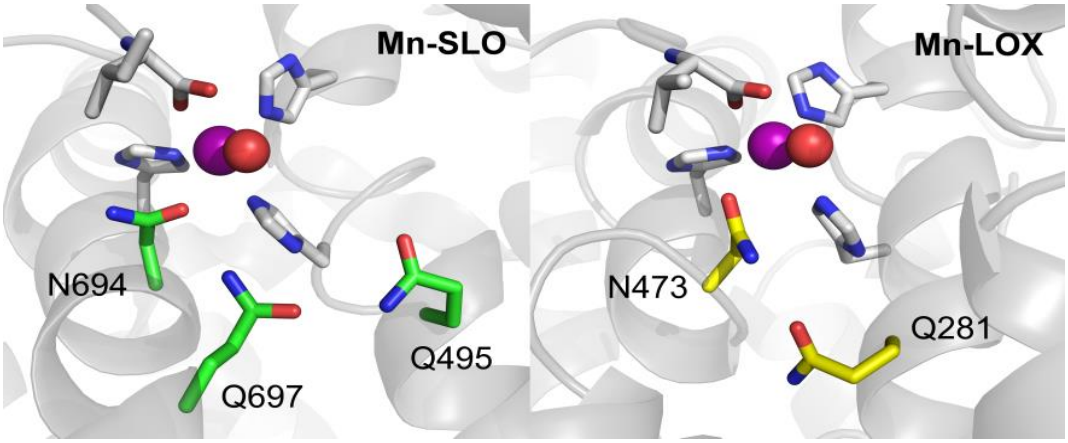

Figure 1.7: *The active sites of Mn-substituted SLO (PDB:3PZW) and MoLOX (PDB:5FNO) contain conserved residues, but the orientations of the primary ligands residues differ slightly; the differences in the second-shell hydrogen-bonding network is illustrated by the color-coded residues (and labeled for reference).*

The orientations of the amino acid residues are suggested to play a role in the reactivities of the enzymes. The standard reduction potentials of Fe^{3+} to Fe^{2+} couple is 0.77 V; the corresponding reduction potential of the iron center in a model plant lipoxygenase from soybean seeds (i.e., SLO) was estimated, using electron paramagnetic resonance (EPR) spectroscopy with redox-active probes, to be ~0.6 V.[29] Conversely, the standard redox potential of Mn^{3+} to Mn^{2+} is 1.5 V, which exceeds the highest redox potential of 1.2 V found in biologics (special pair in photosystem II).[30] The redox potential of manganese within the *Mo*LOX system is currently unknown but is expected to fall within the same range as the iron LOXs. Thus, the local protein environment is expected to play a crucial role in influencing the potential of the metal cluster.

In a recent study, the metal environments of *Mo*LOX, *Gg*LOX, and Mn-substituted SLO were analyzed and compared using cryogenic EPR spectroscopy.[25] In *Mo*LOX, the EPR absorbance spectrum (**Figure 1.8**) is indicative of a typical high-spin (S=5/2) Mn^{2+} cofactor with a large zero-field splitting (ZFS) pattern (i.e., ellipsoid symmetry for electron spin density). *Gg*LOX had a similar EPR spectrum, suggesting a consistent pattern between two different fungal LOXs. Mn-substituted SLO displayed more of an isotropic spin density (i.e., lower ZFS or narrower EPR signal). Thus, these EPR data support the conclusion that the fungal and plant enzymes impose a slightly different local environment accounting for the differences in catalytic properties.

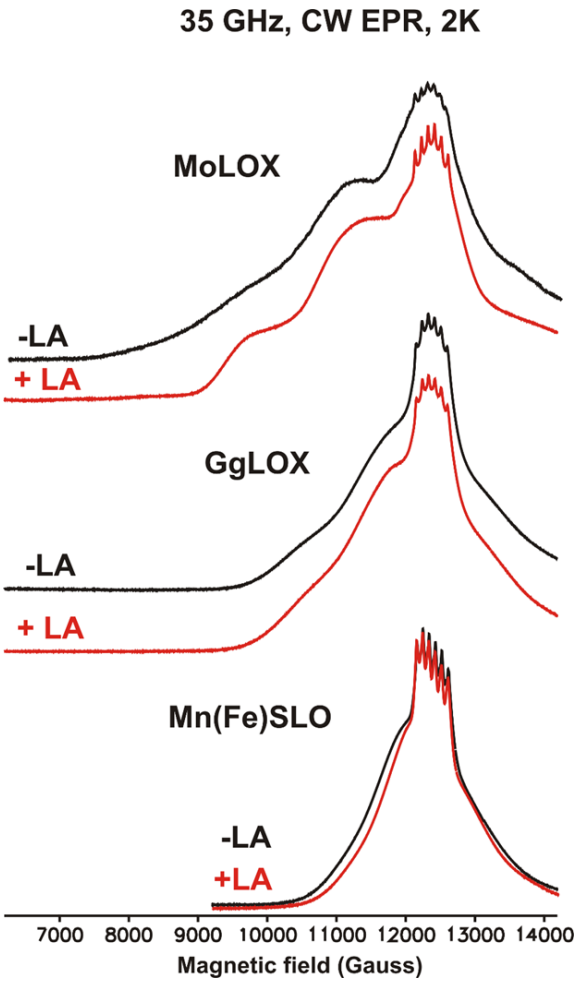

Figure 1.8: *EPR Spectra of WT MoLOX, GgLOX, and Mn-substituted SLO. The samples were analyzed in the presence (red) and absence (black) of LA.*[25]

Electron nuclear double resonance (ENDOR) spectroscopy, a two-dimensional EPR-detected NMR approach, was applied to *Mo*LOX to determine a 3-D structural model of LA binding in the enzyme.[8] Using ^{13}C-labeled substrates, the ENDOR data were extracted and the carbon-11 to Mn and carbon-10 to Mn^{2+} distances were used as restraints in a molecular dynamics (MD) simulation. The resulting model of the enzyme-substrate complex is shown in **Figure 1.9**. From this model, several active site residues were identified to make contact with the substrate. Several alanine site-directed protein variants were constructed at these individual sites

and their resulting kinetics are reported in **Table 1.1**. Importantly, removal of the bulky sidechains of these residues often leads to impairment of activity. Of particular note is the mutation of the conserved leucine clamp residue (L331) to alanine that was associated with a ~18-fold decrease in k_{cat}.[25] The likely reason for this outcome stems from the mutated enzyme not being able to correctly position the substrate for hydrogen abstraction, thus, activity is decreased.

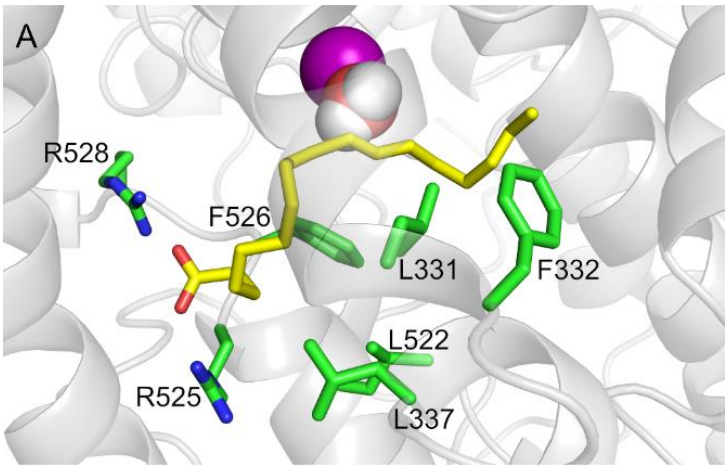

Figure 1.9: *Molecular dynamics model of LA (yellow sticks) bound to active site of MoLOX. Potentially important MoLOX sidechains involved in substrate positioning.*[25]

Table 1.1: *Kinetic parameters of MoLOX active site variants*[a]

*Mo*LOX	k_{cat} (s^{-1})	K_M (μM)
WT	2.1 ± 0.2	14 ± 2
L331A	0.12 ± 0.02	10 ± 2
F332A	0.76 ± 0.03	16 ± 2
L337A	1.9 ± 0.1	9 ± 3
L522A	0.24 ± 0.04	17 ± 8
F526A	0.11 ± 0.01	9 ± 3

[a]Reactions were conducted with LA at 20°C in 0.1 M borate, pH 9 buffer. The kinetic are averages of triplicate measurements collected from one biological sample on three independent days.[25]

1.7 Unique hydroperoxide product

The main product of the *Mo*LOX reaction with LA is a unique bis-allylic 11*S*-HpOD product, which differs from the canonical enzymes that only produce the conjugated hydroperoxides. This product is generated by the insertion of oxygen at the carbon located between two allyls. Then, the fungal LOXs can also produce the 9*S*- and 13*R*-HpOD product through a β-fragmentation mechanism (**Figure 1.10**).[16] How this 11*S*-HpOD product affects plant biochemistry or the enzyme's involvement in cell death (leaf necrosis) is not currently known.

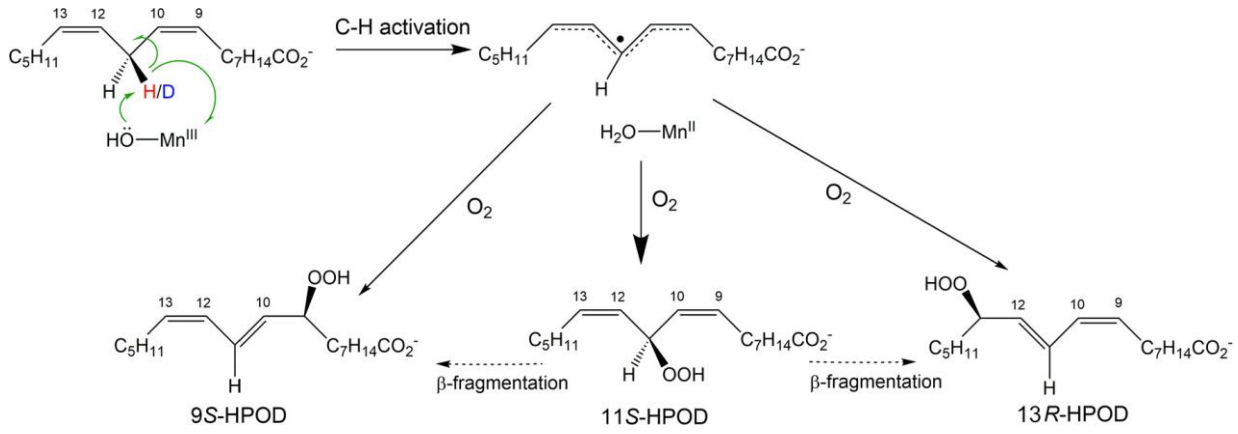

Figure 1.10: *Reaction mechanism for the oxidation of the substrate LA by manganese lipoxygenases. The Mn-LOXs can produce 13R-, 9S-HpODE products or the unusual bis-allylic 11S-HpODE product.*

1.8 A "New" Subfamily of Fungal Lipoxygenases?

A recent bioinformatics study identified a total of 48 potential fungal LOX sequences, including the five previously characterized enzymes.[20] These sequences were divided into three subfamilies based on phylogenetic analysis. The fungal LOXs studied to date are all grouped in a similar family as *Gg*LOX and *Mo*LOX and are considered **class I** or "prototype fungal LOXs." These representatives are well studied and have been established with LOX activity and select systems have been characterized structurally. This class of enzymes is glycosylated, part of the fungal secretome, and have an active Mn^{2+} cofactor.[20]

A second subfamily, or **class II** fungal LOXs, are primarily from pathogens of parasites with a few being from plant pathogens and fungi used for bio control. Of note, these putative LOXs contain a cysteine at the position of the invariant Leu "clamp". There are only nine representatives in this class. The leucine clamp residue assists in positioning the bis-allylic carbons of substrate for hydrogen abstraction to initiate enzyme catalysis.[31] The Leu clamp is conserved in "prototype" fungal LOXs and all canonical Fe-LOXs.[20] This natural substitution in the class II fungal LOXs may be of particular functional interest. Previous leucine clamp residue studies in SLO (residue L546) and *Mo*LOX (residue L331) mutated the residue to an alanine, creating less bulk. These mutations showed significant decreases in activity (*ca.* 20- to 100-fold decreases in enzyme rate).[25,32] While the natural mutation may have functional significance, to-date no class II fungal lipoxygenase has been isolated or biochemically characterized.

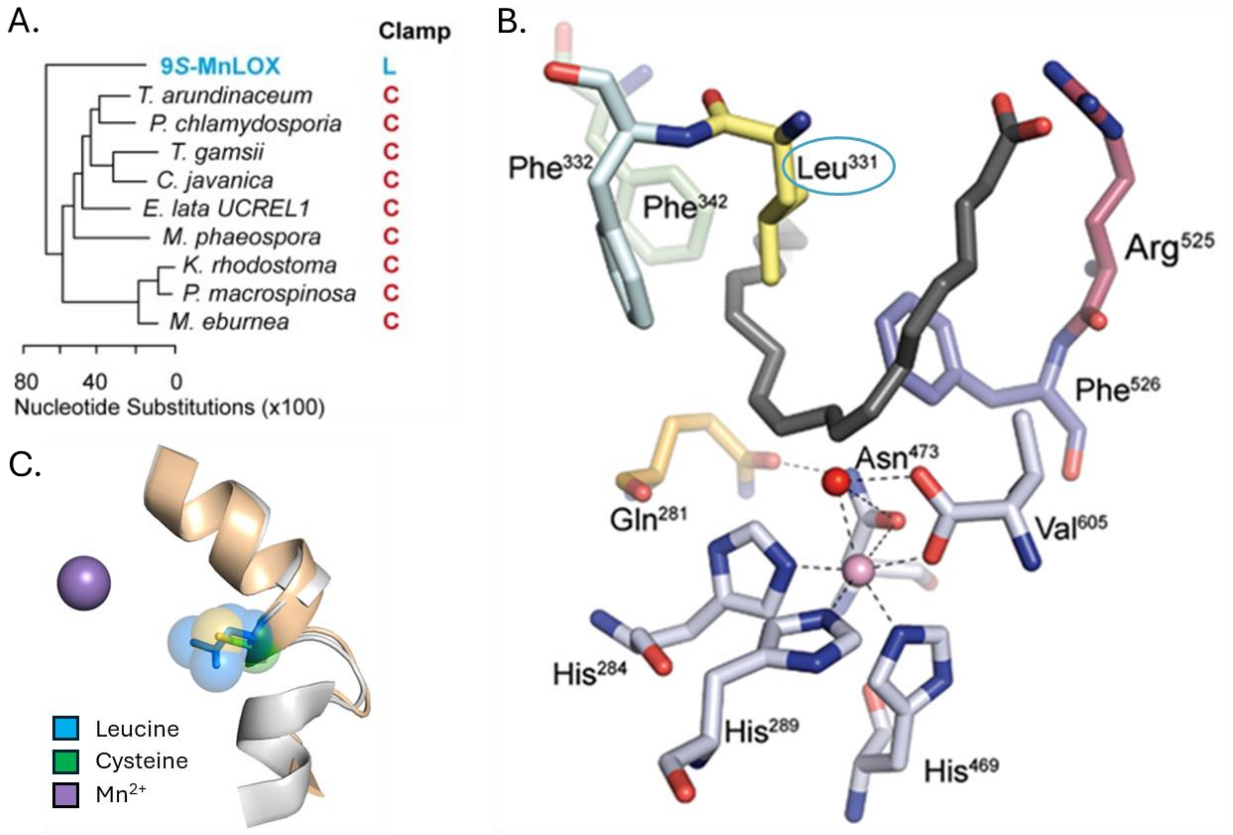

Figure 1.11: *The substrate clamp of class II fungal LOXs is a cysteine instead of a leucine.*[7,20] *(A) Phylogenic tree of Class II representatives. (B) A crystal structure study has shown MoLOX contains the Leu clamp residue.*[7] *(C) Overlay of predicted mutation of Leu clamp to Cys, showing the difference inside chain bulk at the active site.*

These two amino acids – leucine and cysteine – are quite different (**Figure 1.11C**). The most significant difference in terms of substrate positioning is the length of the size chains. Leucine has an isobutyl group side chain, whereas cysteine contains a thiol (-SH) group as its side chain. The isobutyl side chain of the leucine is the portion of the amino acid that provides hydrophobic bulk to position the substrate for effective oxidation by the metal center The thiol side chain is much shorter than a leucine and it also lacks the second "arm" (branch) for holding the substrate in place. Cysteines also have the ability to undergo oxidation in the cell.[33] The role

of this Cys in LOX catalysis and its functional consequences in class II enzymes are not understood.

1.9 Thesis Overview

The goal of this research project is to express, isolate, and biochemically characterize representative class II fungal LOXs *in vitro* using structural and functional studies. This information may help us to understand the evolutionary consequence of a substrate binding site mutation used to position the substrate. Chapter 2 describes the methods of the Thesis, Chapter 3 outlines the major Results, and Chapter 4 presents the Discussion.

Chapter Two

Materials and Methods

2.1 Selection of representative class II fungal LOXs

There are nine predicted class II fungal LOXs, and three were selected in this work for biochemical studies.[20] Those three enzymes are from *Trichoderma arundinaceum (Ta)* (bio control of *B.cinerea*), *Periconia macrospinosa (Pm)* (root-fungus symbiosis), *and Cordyceps javanica (Cj)* (control of Asian citrus jumping plant lice). *T. arundinaceum* is a candidate for further studies due to closely related sequences in the other *Trichoderma* species.[34] *P. macrospinosa* is a mychorriza fungus, meaning it plays a role in root-fungus symbiosis.[35] Many class I fungal LOXs are considered to contribute to plant pathogenesis, so a LOX involved in a plant growth is an interesting purpose. *C. javanica* is a pathogen of insects, which is another difference in target organism.[36]

While all three of these putative class II LOXs have a Cys substituting at the otherwise conserved Leu clamp, there are other sequence variations, including the C-terminal peptide and active site 'Bo1' determinant that may influence the positioning of substrate for oxygen insertion.[37] In addition, these three representatives were selected based on differing number of *N*-linked glycosylation, with *PmLOX* predicted to have the most glycosylation sites of the nine class II fungal LOXs (**Table 3.2**).

2.2 Expression and Purification of MoLOX in Yeast

*Mo*LOX is expressed in the *Pichia pastoris* yeast system. The gene encoding *Mo*LOX was previously synthesized by Genscript in the pPICZα plasmid, in line with the α secretion peptide, which promotes secretion of the protein upon expression. For a given transformation, the yeast strain, *P. pastoris* X33, is transformed using the lithium chloride heat shock method with the SacI-linearized pPICZα plasmid containing the fungal LOX gene. Transformed cells were plated on YPD (yeast extract/peptone/dextrose) plates containing Zeocin antibiotic marker. The plates were incubated at 28-30°C for 3 days or until colonies began to appear. A single colony of these stable cell lines was grown in a starter culture containing BMGY minimal medium (phosphate-buffered yeast nitrogen bases with glycerol) until desired growth was reached. For large scale (4 L) expression, a 200 mL starter culture was grown to OD_{600} (optical density at 600 nm) of 20. The cells were collected by centrifugation, washed in water (to remove glycerol), and resuspended in expression minimal medium of BMMY (phosphate-buffered yeast nitrogen bases with methanol) in baffled flasks. Methanol (0.5% final concentration) induces protein expression. The protein expression takes place for 3-4 days in shaking incubators (30 °C) and was supplemented with fresh methanol (0.5% final concentration) each day.

Because the fungal LOX gene is expressed in line with the α secretion signaling peptide, Mn-LOXs are secreted from the yeast into the media, so the cultures are centrifuged to remove the cells, and the supernatant will be kept for protein purification. The protein was purified using hydrophobic interaction chromatography to capture the protein.[8,16,23] After the cells were harvested, ammonium sulfate was added to the protein containing media to reach a 1 M final concentration, and the solution was neutralized with dropwise addition of 10 M KOH. The media was filtered and loaded by gravity on Phenyl Sepharose (hydrophobic interaction) column

material in an E-cono (Bio-Rad) column. After the protein had been captured, the column was washed with ~5 column volumes (CVs) of high salt buffer (1 M ammonium sulfate and 25 mM potassium phosphate, pH 7). The protein was eluted using a linear salt gradient: 1 M ammonium sulfate and 25 µM potassium phosphate (high salt) and 25 µM potassium phosphate (low salt). A fraction collector collected the eluted protein. The fractions that display enzyme activity and/or show protein absorbance at A_{280} are concentrated using a JumboSep concentrator (30 kDa MWCO) and further purified using size exclusion chromatography (SEC) with an ÄKTA FPLC. The HiPrep S-200 column was pre-equilibrated with 50 mM HEPES (pH 7.5), 150 mM NaCl buffer. The purified protein was collected, concentrated to 0.1-0.2 mM, flash frozen in aliquots, and stored in the -80°C freezer until further use. SDS-PAGE analysis determined the purity of the samples.

2.3 Optimizing Class II Fungal LOX Protein Expressions

Small scale (0.5 L) "test" expressions of Class II fungal LOXs were conducted to determine optimal expression levels of the putative LOXs. The activity of the class II expressions was checked daily (up to 5 days) and compared to a prototype Mn-LOX, such as *Mo*LOX, to understand if these putative LOXs contain LOX activity (i.e., ability to oxidize fatty acids). In brief, the fungal LOX genes were synthesized by Genscript and sub-cloned into pPICZα. The plasmids were transformed into *P. pastoris* X-33 cells and starter cultures were grown as described for *Mo*LOX above. After 3 days, the cells were collected by centrifugation, washed and added to 0.5 L of BMMY media (supplemented with methanol). On the test day, a small aliquot (1 mL) of culture was centrifuged to pellet the cells, the supernatant was mixed with 50

µL of 1 mM LA solution (in 50 mM sodium borate buffer, pH 9.0), and the product formation was tracked using UV-vis spectroscopy in kinetics mode (wavelength, 234 nm).

To estimate the expression levels and protein content from the expression of the class II LOXs, a Bradford assay (using Coomassie Protein Assay Reagent) of the yeast culture media was conducted. In a plastic cuvette, 900 µL Coomassie dye and 100 µL of culture from medium were mixed. The absorbance of the mixture was analyzed using UV-vis spectroscopy at 595nm; the absorbance value and protein content are proportionally related. *Mo*LOX and yeast cells were used as a reference for this assay.

Parameters to optimize protein expression include the number of days for expression as well as the incubator shaking speed. Once these parameters were determined, large scale (4 L, or more) expressions were performed in BMMY media. The proteins were purified as described for *Mo*LOX (above).

2.4 Expression and purification of Soybean Lipoxygenase (SLO) in E. coli

The plasmid containing soybean lipoxygenase (SLO) gene was transformed into *E. coli* BL21 Codon Plus cells and grown overnight at 37°C in LB medium to be used for expression. The cells were divided among four flasks containing 2xYT and supplemented with ampicillin (100 mg/L final concentration) and ethanol (3% final concentration). Ethanol helps promote the co-expression of chaperons to improve SLO expression levels. The expression cultures are placed in an incubating shaker at 37 °C and grown to an optical density (OD_{600}) of 1-1.2, at which point the temperature is reduced to 16-18 °C. The cultures are incubated for approximately 48 hours and harvested by centrifugation.

To purify, the cells are resuspended in a lysis buffer The lysis buffer consists of 16 mL 50% glycerol, 8 mL sodium phosphate buffer supplemented with NaCl (0.5 M, pH 8), 4 mL $MgSO_4$ (20 mM), 20 mg AEBSF (4-2-aminoethyl benzenesulfonyl fluoride) hydrochloride, 0.9 mL 10% tween-20, 4 µL Benzonase™ nuclease solution (25 KU/µL) and 2 µL rLysozyme™ solution (30 KU/µL).[38] When the mixture of the buffer and the cell pellet became homogenous, the solution was sonicated for three 5-minute cycles with a 5-minute rest in between each. The disrupted cell suspension was centrifuged to remove the cellular debris. The sample is added to dialysis tubing and dialyzed in 20 mM Bis-TRIS (pH 6) overnight at 4 °C. On the next day (day 2), the dialyzed product was centrifuged to remove any extra cellular debris and loaded to an SP cation exchange column. The column was washed with 2 CV of 20 mM Bis-TRIS (pH 6) and the protein was eluted using a gradient from 0 to 500 mM NaCl in 20 mM Bis-TRIS and collected by a fraction collector. The fractions are checked for protein presence by a UV-vis spectrometer (A_{280}). A small aliquot of the peak fractions was collected and used for SDS-PAGE analysis. The collected fractions were added to dialysis tubing to again be dialyzed in 20 mM Bis-TRIS (pH 6) overnight. For day 3, the sample was centrifuged to remove excess debris. The supernatant was loaded to a UnoS cation exchange column and eluted using a gradient mixer as described for the SP column. The eluate was collected by a fraction collector and checked for the presence of protein. A small aliquot of the peak fractions was again collected for SDS-PAGE analysis. The collected fractions were added to dialysis tubing and dialyzed for a final time in a 0.1 M borate buffer overnight. The protein was concentrated to 50-100 µM, divided into 50 µL aliquots, flash frozen, and stored in a -80 °C until needed.

2.5 LOX Mutant DNA Preparation

Mutants of SLO (L546C, L546S), *Mo*LOX (L331C), and *Ta*LOX (C309L) were prepped using site directed mutagenesis with the Qiagen QuickChange kit. Polymerase chain reaction (PCR) was conducted under the following conditions: 1.) 98 °C for 30 sec, 2.) 30 cycles of 98 °C for 10 sec, 60 °C for 30 sec, and 72 °C for 5 min, and 3.) 72 °C for 10 min for termination. The mutation sequences were analyzed and confirmed.

2.6 Expression and Purification of TaLOX into E. coli

To express *Ta*LOX in *E. coli*, the gene was sub-cloned into a pET28a vector with an encoded N-terminal His-Tag. The plasmid was transformed into *E. coli* BL21 Codon Plus cells and a starter culture was grown in LB overnight at 37°C. The cell culture was divided equally into 4 flasks containing 2xYT and 500 µL kanamycin. The cells were grown in a shaking incubator at 37 °C to and OD of ~0.8, where the temperature was dropped to 17 °C. Then, 0.1 mM isopropyl β-D-thiogalactopyranoside (IPTG) was added to each flask for induction. After 48 hours, the cells were harvested using centrifugation. The cell pellet was collected.

For purification, a lysis buffer was prepared to remove the proteins from the *E. coli* cells. To further disrupt and break up the cells, sonication was used. The sonicated sample was centrifuged to remove the cellular debris, and the supernatant was collected for gravity column purification. A Ni-NTA column was used to capture the His-Tag on the *Ta*LOX. This process allows any unwanted protein to pass through the column and into the flow through. The column was washed using Buffer A (20 mM Tris, 20 mM imidazole supplemented with 0.5 M NaCl, pH 8) to remove non-specifically bound protein from the column. The enzyme was eluted from the

column to a fraction collector using Buffer B (20 mM Tris, 200 mM imidazole supplemented with 500 mM NaCl, pH 8). The fractions were analyzed for protein content through UV-vis and collected to concentrate. The sample was concentrated using a 30 kDa MWCO concentrator to 2.5 mL for buffer exchange. The concentrated sample is loaded onto a PD-10 column equilibrated with 50 mM HEPES (pH 7.5), 150 mM NaCl buffer. Five 1 mL fractions were eluted with the equilibration buffer and collected from the column. Protein content was analyzed using UV-vis. The protein was aliquoted as necessary and stored in a -80 °C for future use.

2.7 Kinetics using Oxygraph+ O_2 electrode

To kinetically analyze the purified LOXs, a Hansatech Liquid-Phase Oxygen Electrode and Oxygraph+ system was used. This system uses an S1 oxygen electrode disc consisting of a platinum cathode and silver anode set into an epoxy resin disc. The disc coupled with an electrode control unit provides an efficient and accurate method of measuring changes in oxygen uptake or evolution. The oxygen electrode was used to test LOX activity of the class II LOXs, through the consumption of molecular oxygen as the second substrate of the LOX reaction. *Mo*LOX was used as a reference.

A salt bridge is created on the oxygen electrode disc to connect the cathode and anode. Instrument calibration is two step with water being an initial standard and a zero-oxygen mixture (water and sodium hydrosulfite) used to adjust the output to zero. In a typical experiment, the buffer and substrate are added to the chamber first, the kinetic run is started on the program, and then the protein sample is loaded to ensure the full measurement is recorded.

The kinetics were performed in steady state at 25 ℃ as a function of substrate concentrations (when applicable): 100, 50, 30, 15, 5, and 2 µM (final concentration) LA. *Mo*LOX data was collected in triplicate. All kinetic data was analyzed using IGOR Pro. The data was plotted (rate versus substrate concentration), and the curve was fitted using the Michalis-Menton equation to obtain k_{cat} and K_M. For class II fungal LOXs the concentration of enzyme used was increased during the trials for improved signal. The substrate concentration was maintained at 100 µM. Different substrates were also tested for specificity (arachidonic acid and α-linolenic acid).

2.8 Metal analysis of class II Mn-LOXs by Inductively Coupled Plasma Optical Emission Spectroscopy (ICP-OES)

ICP-OES is a method used to detect and quantify trace amounts of metal in a solution sample. Class II fungal LOX samples were analyzed using ICP-OES in the Chemistry department at Virginia Commonwealth University (VCU). Standards containing iron, manganese, and copper were prepped the day of testing and of the concentrations 0 (blank), 25, 50, 100, 250, 500, and 1000 ppb. The LOX samples were prepared with an expected 500 ppb metal concentration range as follows: nitric acid was added (to 2% final concentration) to denature the enzyme; the protein samples were briefly centrifuged, and the supernatant was transferred to a fresh tube. The ICP-OES method was created to detect copper (324, 327nm), iron (238 and 260 nm), and manganese (258 and 259 nm) at the highest detection wavelengths while avoiding spectral overlap; furthermore, the two highest detection wavelengths were used to corroborate anomalous results from interference. The raw data was converted to ppb to µM based on the molecular weights of the metal, and then, to a ratio of protein to metal.

2.9 Ferrozine assays for iron content analysis

Ferrozine assays were used to measure iron content in SLO and *Ta*LOX expressed in *E. coli* samples. The method uses iron standards and ferrozine chelator prepared samples. The iron standards were prepared at 0, 10, 25, 50, 100 µM at 100 µL volumes. The LOX samples were prepared at 100 µL of 50 µM. The LOX samples and iron standards were treated identically. The protein is denatured and treated with a reductant to generate Fe^{2+}. Ferrozine was added to the solution and binds to the free Fe^{2+}. This compound is visible at 562 nm. A slope was generated from the iron standard absorbances and used for calculating iron content of the samples. The absorbance values of the samples are corrected to match the blank.

2.10 Kinetic Analysis of Soybean LOX Mutants using UV-vis spectroscopy

To characterize the hydrogen transfer and tunneling efficiency of the SLO mutants, steady-state kinetics is measured using UV-vis spectroscopy. The wavelength is set at a fixed 234 nm to capture the absorbance of the conjugated hydroperoxide products produced by SLO. The reactions were initially performed at 30 °C across different linoleic acid substrate concentrations (100, 50, 25, 20, 10, 5 µM). Deuterated linoleic acid is used to determine the kinetic isotope effects (KIEs) - the comparative rate of H vs the rate of D transfer. All SLO variant kinetic data was collected in triplicate and analyzed using IGOR Pro as previously mentioned (section 2.7).

2.11 *DeepMind AlphaFold 3 for protein folding predictions*

DeepMind is an artificial intelligence company operating under Google, and recently it released the server AlphaFold 3 (AF3).[39] This server is able to take a protein sequence and predict the tertiary and quaternary structure; this version has improved over the AF2 platform as it can also predict metal binding sites. Crystal structures are not easy to obtain due to factors such as cost and growing crystals; therefore, using AI to generate protein structures could aid in predicting function and giving a visualization of the protein at hand. AF3 can analyze proteins, DNA, RNA, ligands, and ions, along with some post translational modifications. The system also reports confidence metrics. The metric pLDDT is a per-atom confidence estimate where a value closer to 100 indicates a higher confidence in the location of the atom(s). The pTM and ipTM scores are predicted template modeling scores used to measure the accuracy of the entire structure. A value between 0.6-0.8 is a gray region meaning the prediction could be correct or incorrect, and a value above 0.8 represents high-quality predictions.

A bonus of using AF3 in this situation is that there are crystal structures of multiple fungal LOXs in the protein database.[7,28] A generated structure like crystal structures will provide valuable information for future questions. The models are aligned in PyMOL, and the program provides a root-mean-square-distance (RSMD) value to estimate the similarity between overlayed structures; a value below 2 Å is generally accepted as similar, and the closer the value is to zero, the better aligned the two structures are. For the crystal structure of *Mo*LOX and the AF3 model, the RMSD value was 0.271 Å.

2.12 Circular Dichroism (CD)

CD experiments for structural information were conducted on a Jasco J-815 CD Spectrometer. The SLO and fungal LOX samples were prepared at a concentration between 1.5-3 µM in 25 mM potassium phosphate (pH 7). The samples were analyzed at 20 °C in the range of 190-250 nm with a scan rate of 50 nm/min. Samples were placed in a Starna cell (path length of 0.1 cm). Digital Integration Time (D.I.T.) is the amount of time the data is integrated over. The S/N is proportional to the square root of the response, so a longer D.I.T. results in a better S/N. In this case, the D.I.T. was 8 seconds. The High Tension (HT) Voltage was monitored during the studies. An HT value higher than 700 V is indicative of not enough photons being sampled by the photomultiplier tube (PTM), meaning the data is not reliable at that point. The concentrations were adjusted when necessary. These experiments were performed in triplicate.

2.13 Differential Scanning Calorimetry (DSC)

DSC experiments were conducted on a TA-instruments Nano-DSC microcalorimeter. The various SLO and *Mo*LOX samples were prepared at 30-40 µM concentration in 50 mM HEPES (pH 7.5) with 0.15 M NaCl. The DSC experiments measured 30-80 °C (heat only) at a rate of 1 °C min^{-1} with a constant pressure of 3 atm. The data was analyzed using TA Instruments NanoAnalyze software.

Chapter Three

Results

3.1 Optimal Protein Expression Tests and Purification

LOX activity in the small-scale yeast cultures used to express the representative class II LOXs was tested with UV-vis spectroscopy in single wavelength kinetics mode at 234 nm. The conjugated hydroperoxide product for the reaction of LOX with polyunsaturated fatty acids is being measured at this wavelength and has a molar extinction of 23.6 mM^{-1} cm^{-1}. Conversely, the substrate, linoleic acid (LA), does not absorb light at 234 nm. The protein in the secreted media is at sufficiently low concentration and therefore does not contribute significantly to the absorbance at 234 nm for these assays.

The reaction of culture media containing *Mo*LOX with LA shows a lag phase in the kinetic spectra (**Figure 3.1**) because of the initial production of the unique 11*S*- bis-allylic product, which does not absorb at 234 nm. That product undergoes β-fragmentation to create the conjugated products (9- and 13-HpOD), which do absorb at 234 nm. An increase in the absorbance as a function of time demonstrates the activity of the enzyme; therefore, it confirms the presence of the expressed enzyme. Further, the MoLOX activity appeared to be maximal at either day 3 or day 4 post induction in the baffled flasks with BMMY media. The activity of the class II fungal LOXs were tested in a similar manner after day 3 and day 4, post inductions. When expressing the class II fungal LOXs, the activity traces were nearly identical for each day. Day 4 was chosen to match that of *Mo*LOX, which clearly demonstrates activity on day 4. Compared to the *Mo*LOX expression cultures, the activity of the cultures from *Ta*LOX, *Pm*LOX, and *Cj*LOX expressions were considerably low or even zero (**Figure 3.1**). *Ta*LOX was the only

one of the three class II fungal enzymes to have increased activity between the two days. The proteins exhibiting low activity can be indicative of i) low protein expression levels, ii) production of only the bis-allylic hydroperoxide product, iii) poor enzyme activity, and/or iv) non-LOX activity/reaction.

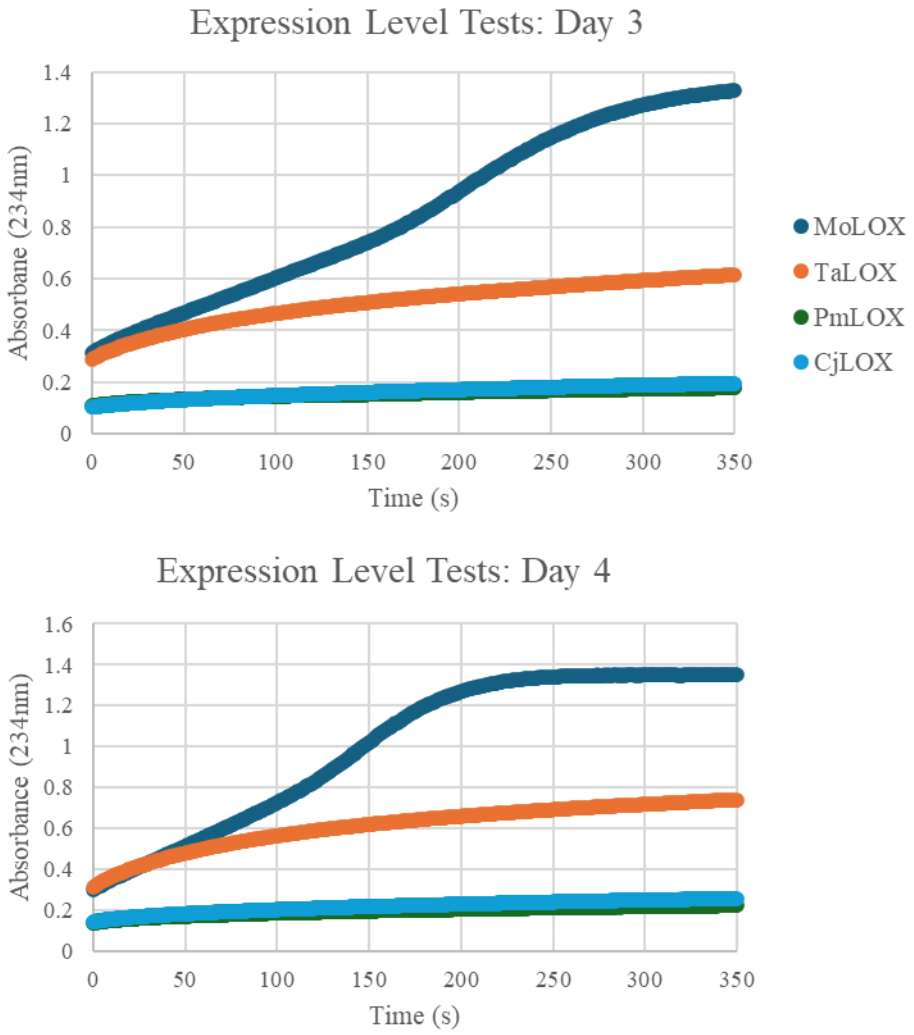

Figure 3.1: *Representative kinetic traces of kinetic activity of MoLOX and class II LOX media in borate buffer and using the substrate LA (50μM). The reactions were run at room temperature.*

To determine the amount of protein produced in the expression media, expression levels of class II LOXs were also analyzed using a Bradford Assay. In brief, the Coomassie dye reagent reacts with the amino acids present in the sample, so the higher the absorbance, the more protein assumed to be present.

The Bradford Assay was only performed for day four of the incubation period to gauge protein content (**Table 3.1)**, where the *Mo*LOX was shown to express optimally based on the kinetic assay described above. When standards (usually BSA) are applied, this assay provides insight on the concentration of net protein expression levels and is therefore not specific to LOX. However, LOX is the primary enzyme secreted in the media and the yeast cells were removed by centrifugation prior to the Bradford Assay, so this assay should provide a relative metric for LOX production. The x33 cells (yeast with no transformed LOX gene) are used as the reference in this case, for it's the system that the proteins are expressed in but should reflect the baseline amount of non-LOX protein produced by the yeast strain. The absorbance from the cells was treated as a zero in this case, with any value above that being protein expressed and secreted from the cells. Noticeably, the class II fungal LOXs yield a higher absorbance value than both x33 cells and *Mo*LOX (in media). This finding suggests proteins are being expressed and secreted from the yeast cells. The class II fungal LOXs are of similar size to the sequence of *Mo*LOX, so the difference in absorbance is not from the proteins being larger or containing more amino acids. Note that this assay does not indicate if the proteins are well folded or active.

Table 3.1: *Representative Bradford assay protein expression level test of class II LOXs from growth media*

Protein Sample	Abs (Day 4)
x33 (cells)	0.532
MoLOX	0.618
TaLOX	1.211
PmLOX	0.809
CjLOX	0.998

3.2 Theoretical mass and predicted glycosylation of class II fungal LOXs

The molecular weight and length of proteins can be used to make inferences on their sizes, shapes, and behaviors. In this case, with the putative LOXs, we can use this information to further infer on the relationship between them and prototype fungal LOXs. The theoretical mass of *Mo*LOX is approximately 67 kilodaltons (kDa), and the class II LOXs are slightly smaller, being within about three kD from the standard Mn-LOX. The amino acid length and molecular weight of the enzymes are all within a 30 amino acid and 4 kDa range, though the percent identities of the class II fungal LOXs are about 40% that of prototype class I fungal LOX, *Mo*LOX (**Table 3.2**).

Table 3.2: *Table of predicted data from the sequences of MoLOX and three class II fungal LOXs. The weight is predicted by ProtParam, the glycans are predicted by NetNGlyc, and the percent identity is from NCBI Blast.*

Enzymes	Length	Weight (kDa)	Glycans	Percent Identity
Magnaporthe oryzae	604	67.0	7	100%
Trichoderma arundinaceum	585	65.0	2	42%
Periconia macrospinosa	595	66.6	7	39%
Cordyceps javanica	575	63.9	2	40%

To date, all class I fungal LOXs are isolated as glycoproteins, with several N-linked post-translational modified carbohydrates appended to their surface. Thus, I analyzed the predicted glycosylation of the class II fungal LOXs to help understand the structure and function of the enzyme.[14] NetNGlyc is a server used to predict glycan presence using a protein primary sequence. The response given is the sequence, where the glycans would be observed, and a table with a likelihood prediction (**Figure 3.2**). Using *Mo*LOX as an example, the server predicts eight glycans in the sequence of the enzyme; the presence of these glycans has been observed in gels by the increased *apparent* molecular weight and smearing of the band. Secondly, EndoH and PNGaseF (endoglycosidases used to remove glycans) reactions of *Mo*LOX causes the protein to migrate in the SDS-PAGE at the predicted molecular weight.[8]

*Pm*LOX is the only class II fungal LOX to contain a handful of predicted glycans with seven glycan locations (**Table 3.2**). *Ta*LOX and *Cj*LOX sequences are only predicted to have two glycans each, with both being early in the sequence. To check for glycosylation, SDS-PAGE was used during the final purification step to analyze for smearing and molecular weights more than the theoretical.

```
Name:  MoLOX    Length:  619
MRVLVWIAGLAPLAVAVPSSSYRVAVAARADNTSASVAPSQNVSGAAPPELVVYTLPCEDGNSTARTAEIRLKQATLLYG      80
PSLLGNASYFPGGPLGDAISLRDQTVWEGAAVVQSLRAFTDAAKVAANIKQNGGLNSLDDFKVLYQDGWKGSVPQGIARG     160
QSENYTSDLLFSMERLSVNPYILKRLHPTEDALPFQVDRATVKQLTKTSLKALHAAGRLFVADHSYQRNYTRLANRYSAA     240
CTALFYLDPRSNQFLPLAIKTNVGADLTYTPLDTDNNNWLLAKIMFNNNDLFHGQIFHVAYPHAIAEIVHLAALRTMSAR     320
HPVLALMERLMYQAYAVRPLGERVLFNKGGLFEQNFAYPQDMVYKFVGDSYPTTGRWRAGYLDTDVRARGLVDADYGPEL     400
PHFPFYEDGSRLVEVIRRFVRSFVDATYHESDEMVAKDAELQAWVAEANGPAGVEDFEPGPLDTRERLVEVLTHMAWLTG     480
CAHHVLNQGEPVTASGVLPMHPTALYAPVPTSKANTTADLLGYLPSAQKSVDQVTLLARFNRPDVVPTNQTLRYMFAAPQ     560
LLLGNGEAYRRANQRFVRAMGRISDEVKARRFDDRGLSQGMPFIWQALDPGNIPFYLSV
..............................N.........N...................N..................      80
.....N.....................................................................................     160
...N.....................................................................N...........     240
...........................................................................................     320
...........................................................................................     400
...........................................................................................     480
................................N..........................................................     560
.....................................................                                       640

(Threshold=0.5)
---------------------------------------------------------------------
SeqName      Position  Potential   Jury    N-Glyc
                                 agreement result
---------------------------------------------------------------------
MoLOX         32 NTSA   0.6857     (9/9)   ++
MoLOX         42 NVSG   0.6709     (7/9)   +
MoLOX         62 NSTA   0.6010     (8/9)   +
MoLOX         86 NASY   0.6908     (9/9)   ++
MoLOX        164 NYTS   0.7453     (9/9)   ++
MoLOX        229 NYTR   0.5192     (5/9)   +
MoLOX        515 NTTA   0.5139     (5/9)   +
MoLOX        549 NQTL   0.4706     (4/9)   -

Name:  TaLOX    Length:  602
MKAQAACLLLNSLALVAEAAPHQWQAVARQGVSQASLPQNDRDRKARAAEVAARNVGFVYGPSLIGEAAPFPNGTLGNAL      80
TQSDMDLWSVDRDDIDSRIMSDVAAIKPAIAANGGLKSLDDYANVLYQGQWKNANPRGVAPGIMTNYTQDLLFSMERLSQ     160
NPYSLVFLKPSDELPFALDDDTTRKIAGATLEELHASSSLFFVDYSWQSELPKTTVAPQRYGAASSAYFYLHPESKDFLP     240
LAIKTNAGKDLIYTPLDSDNDWLLAKMIFNVNDLFHSQMLHLVITHDVSEAVHEAALHTLSPKHPVMVILDRLMLQAYSS     320
RIVGEELCFNPGGHWDQLMYINNDGCRDYVTQTWPTSGRFQAGYLHTDLKARGLINDQGEYPFKAFPFFQDASEIHDAYR     400
AFFQSFVDSYYASDKDVVADWEVQSWFIEATARAQVQDFPKASPASPVTKDTLVDVLTHFGFIVSVGHHALNGGDPVGSK     480
ATLPFHLPALYAPLPEAKGVTDLIPFLPPAANAIQYIGFIASFNRPFYETSDRTLKAAFSEDSMLAKLNKETNDAASEFV     560
NSMQDLSNRVRSRGFDENGLSMGMPFVYRTLDPNYIPFFCAV
.....................................................................N.......      80
.............................................................N.............      160
...........................................................................................     240
...........................................................................................     320
...........................................................................................     400
...........................................................................................     480
...........................................................................................     560
.....................................                                                       640

(Threshold=0.5)
---------------------------------------------------------------------
SeqName      Position  Potential   Jury    N-Glyc
                                 agreement result
---------------------------------------------------------------------
TaLOX         73 NGTL   0.6711     (9/9)   ++
TaLOX        146 NYTQ   0.7669     (9/9)   +++
```

Figure 3.2: *Output received from NetNglyc server with MoLOX (top) and TaLOX (bottom). A potential value higher than a 0.5 is considered a likely location of glycosylation.*

3.3 Purification results

SDS-PAGE is the final step of purification, and it serves to identify purity of the sample, and presence of glycosylation for fungal LOXs. The purity of the sample is seen by the presence of a single band in the gel. The weight of the enzyme is shown where there is one solid band in a set location from the marker. For example, *Mo*LOX is predicted to weigh around 70 kDa, but the band instead migrates at a much higher mass of ~100-120 kDa based on the standard markers and the band "smears" down the gel. This smearing is caused by heterogenous *N*-linked glycans on the sample protein. Removal of the glycans by endoglycosidase H (endoH) results in a new migration pattern for MoLOX with a mass of ~70 kDa, consistent with the theoretical mass of the protein. Two class II fungal LOXs, *Ta*LOX and *Pm*LOX, as isolated from *P. pastoris* cultures (in a similar manner to *Mo*LOX) migrate to their calculated weight and don't show the smearing effect (**Figure 3.3**). This suggests that these enzymes are not experiencing the PTM glycosylation.

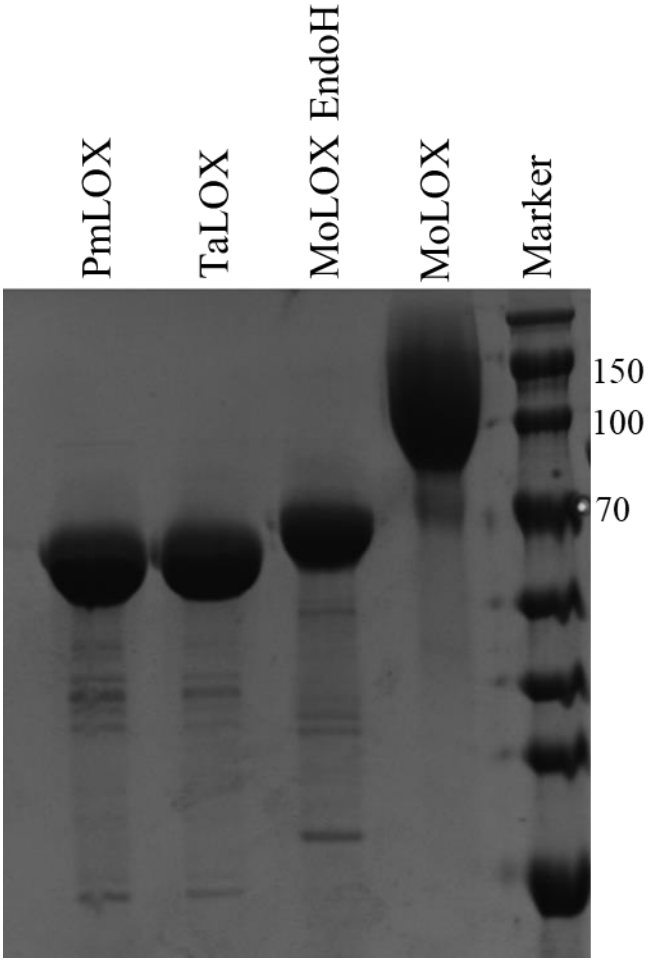

Figure 3.3: *SDS-PAGE of MoLOX, with and without glycans (EndoH is used to cleave the glycans), and two representative class II fungal LOXs - TaLOX and PmLOX.*

*Ta*LOX has a predicted weight of 65 kDa (**Table 3.2**), and it migrates just shy of 70 kDa (**Figure 3.3**), suggesting that it does not contain PTM glycans. To probe this possibility further, the presence of glycans was also tested by treating *Ta*LOX with EndoH and PNGaseF as previously done on *Mo*LOX, and the samples were run on an SDS-PAGE gel.[8,23] Each of the three samples, TaLOX (as isolated) and the two treatments, migrated identically. Thus, the result

of the treatments further corroborated the conclusion that class II LOXs express and isolated from P. pastoris without glycosylation (**Figure 3.4**).

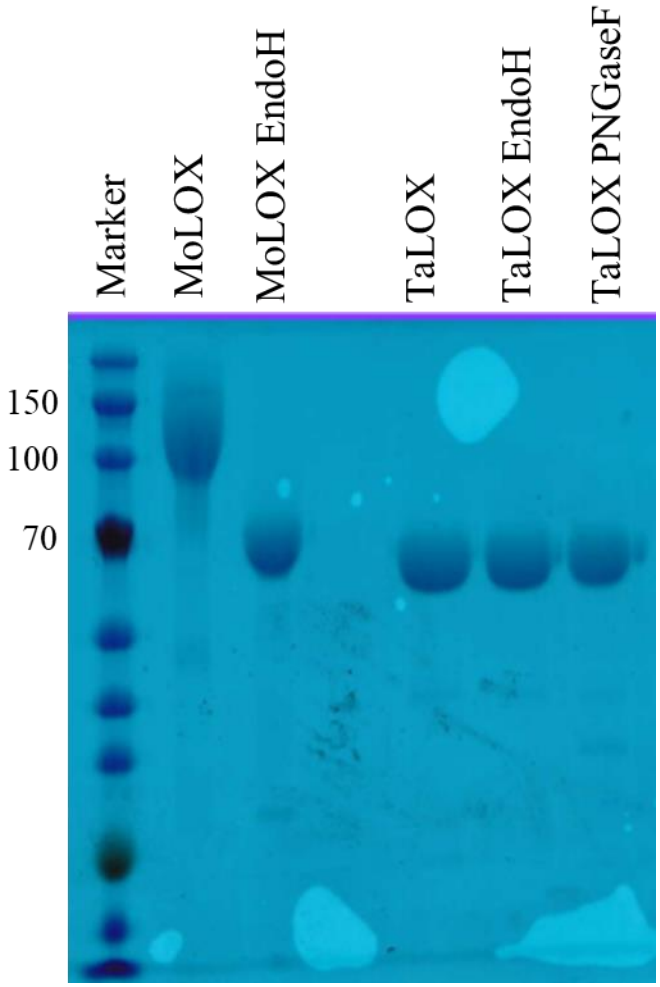

Figure 3.4: *SDS-PAGE gel of MoLOX with and without glycans and the attempt to remove potential glycans from TaLOX using EndoH and PNGase F.*

3.4 Kinetics of MoLOX and representative class II fungal LOXs on O_2 Electrode

The main product of the *Mo*LOX reaction with LA is a unique bis-allylic 11S-HpODE product. This product does not absorb near UV light; thus, the enzymatic activity is analyzed using an O_2 electrode to track the rate of oxygen consumption. The oxytrace+ program outputs

this value of oxygen in the sample in nmol/mL. To start, the reaction of buffer and substrate was run to analyze an oxygraphy trace without enzyme to serve as a blank (**Figure 3.5**). Auto-oxidation may occur during a reaction. The reaction shows very little change in rate and does not run to completion (a dip in runs to a plateau). The reaction of *Mo*LOX (0.25 µM at 25 °C, 100 µM concentration of LA, pH 9.0) is used as a reference for potential LOX activity within the class II fungal LOX samples. *Mo*LOX has a trace that begins to slowly decrease (lag phase) when the enzyme is added to the solution, and the rate is linear until the substrate is used up, where it plateaus (**Figure 3.5**). These reactions range in time depending on temperature and concentration of enzyme or substrate. A slightly noticeable difference between the blank reaction and the *Mo*LOX appears at the beginning of the trace with the addition of enzyme. In the enzymatic reaction, the instrument clearly recognizes the addition of *Mo*LOX with a slight alteration in the trace before the reaction then takes place.

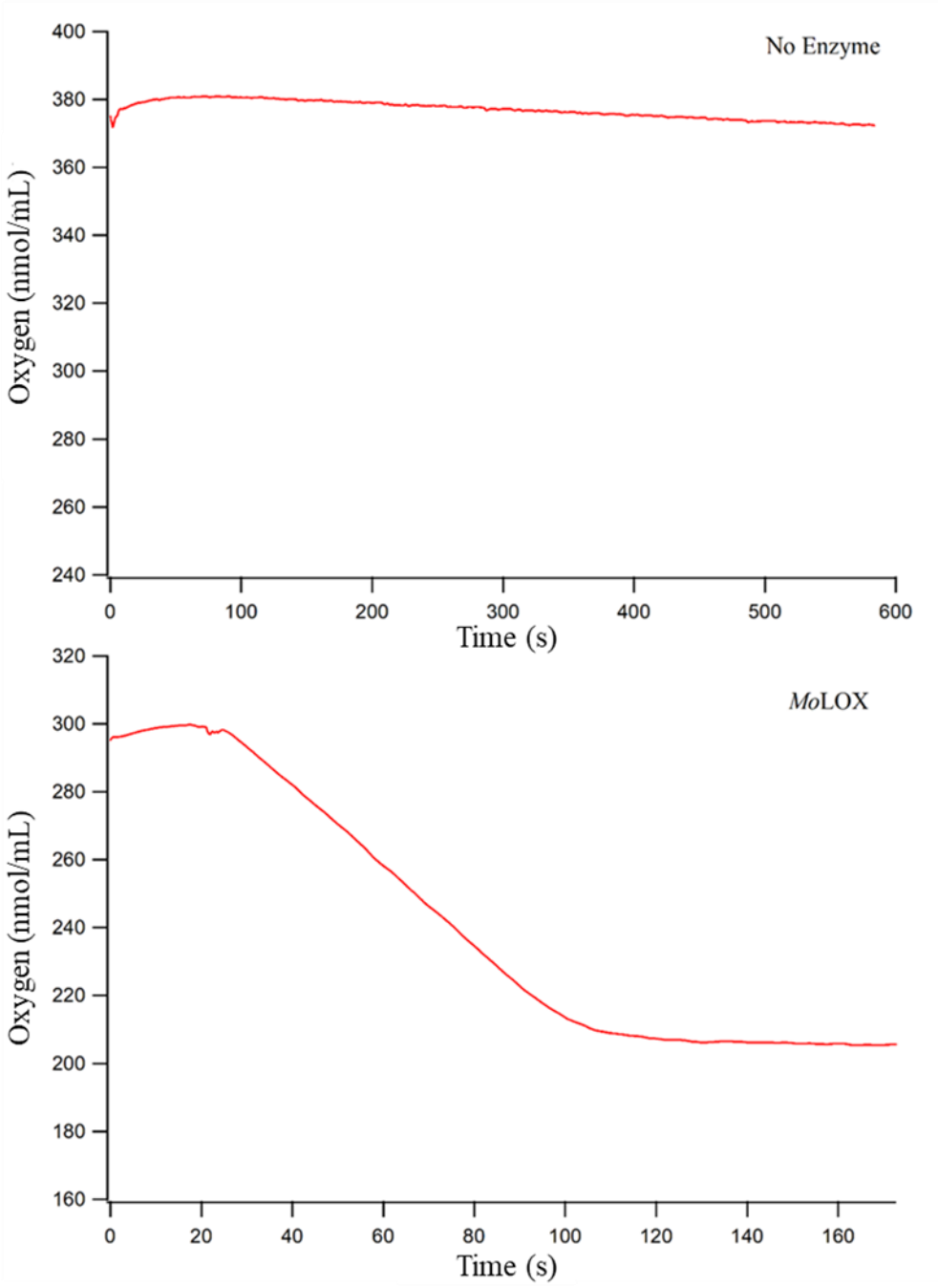

Figure 3.5: *Representative Oxygraph of LA oxidation at 25 °C: (top) without and (bottom) with 0.25 µM (final concentration) enzyme. The substrate concentration was 100 µM.*

Lipoxygenases oxidize fatty acids, and each LOX can have a preferred substrate; however, the LOXs can be active at different pHs.[23,40,41] The *Mo*LOX reaction with LA was previously shown to be active across pH 7 to 9.[23] *Ta*LOX reactions with LA were collected at both pH 7.0 and 9.0. The reaction at pH 7.0 yielded a noisy oxygraphy signal with effectively zero rate of oxygen consumption (i.e., flat trace), whereas the reaction with pH 9.0 was a low S/N trace with some signs of activity during a 4-minute measurement (**Figure 3.6**). The beginning addition of enzyme at pH 7.0 jumped between 10 nM in O_2 consumption rate rate, whereas at pH 9.0, the addition of 4.5 μM *Ta*LOX enzyme produced a non-zero dip in O_2 concentration, but the O_2 consumption rate stayed within 5 nM. For comparison, ~100 nM rates were observed for the same timescale with 0.25 μM *Mo*LOX enzyme. Further pH tests were not necessary with this information, for both *Ta*LOX and *Mo*LOX appear to function better at pH 9.0, which is clear of the CMC. Thus, further reactions were carried out at pH 9.0, including for the other class II fungal LOXs.

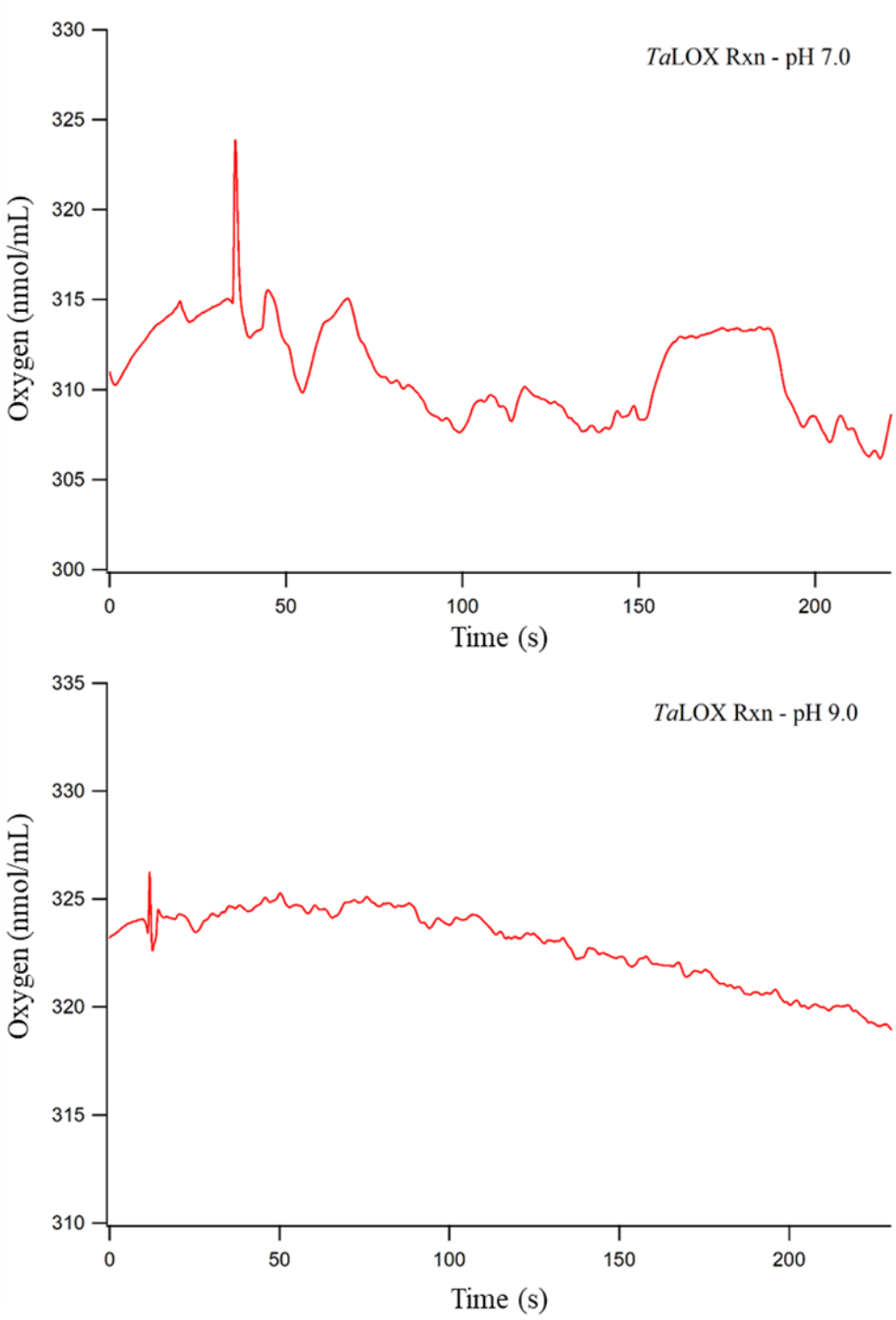

Figure 3.6: *Oxygen electrode trace of TaLOX and pH preference reactions. The two pHs used are 7.0 (top) and 9.0 (bottom). The reactions used 100 µM LA and 4.5 µM enzyme at 25 °C.*

Alongside determining the optimal pH of the class II fungal LOX enzymes, various substrates reactions were used for substrate specificity studies (**Figure 3.7**). Using LA and αLA, the enzyme demonstrated low, albeit some, activity. The corresponding rates showed that αLA was half as efficient as LA, but there was some oxygen consumption during the trial. Arachidonic acid yielded a noisy signal when used; furthermore, the reaction never completed the typical trace pattern shown by LOX species, being nearly linear. This finding led to the continued use of linoleic acid as the primary substrate being used when analyzing the kinetic activity of class II fungal LOXs.

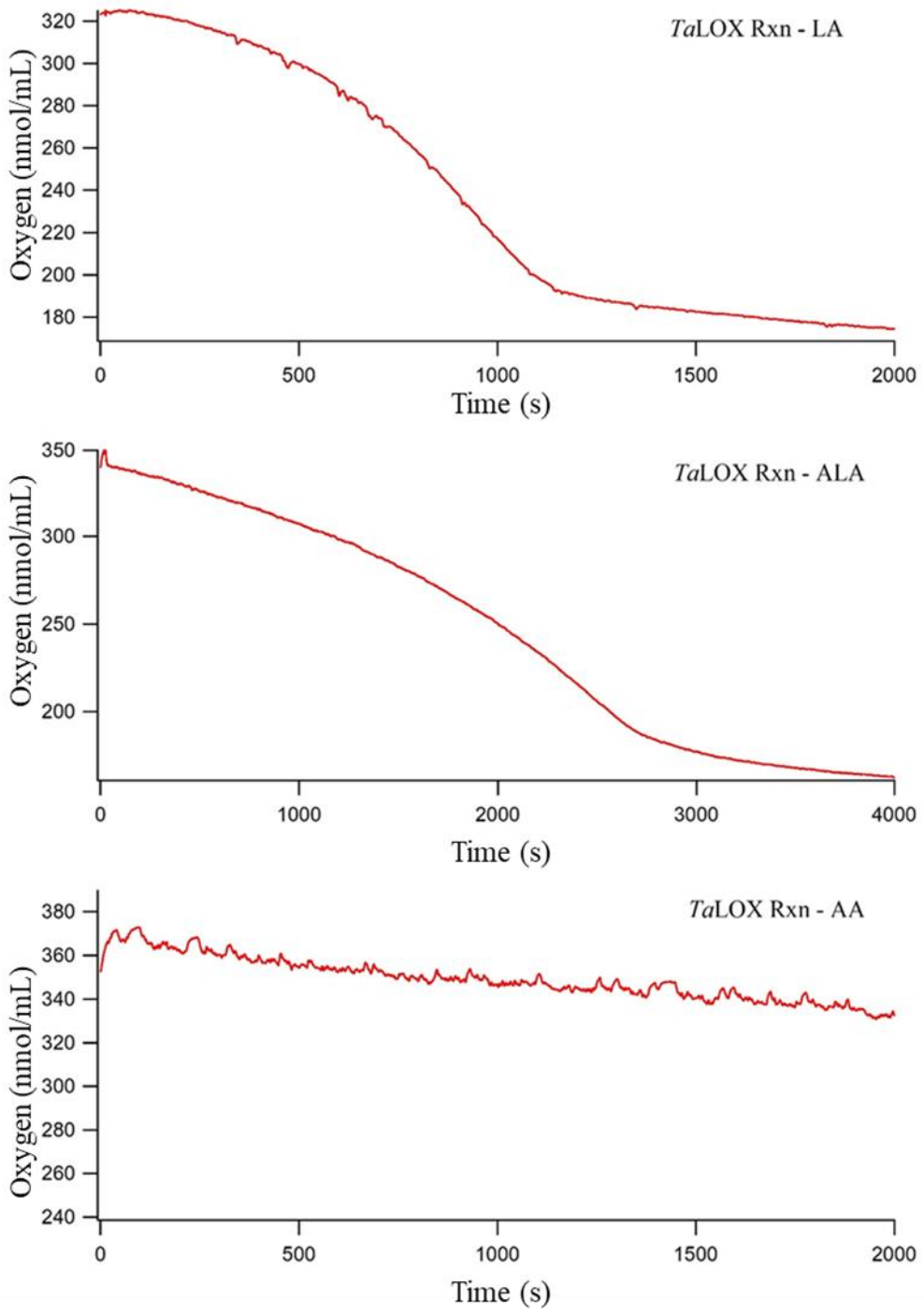

Figure 3.7: *Substrate specificity studies of TaLOX. Each reaction used 4.5 µM enzyme and 100 µM LA. Temp = 25°C. Buffer, 0.1 M borate pH 9.0.*

For the class II fungal LOXs, various concentrations of enzyme were used to obtain a value for the rate. The three volumes used were 2.00, 10, and 30 µL. The concentration of the enzyme within the reaction varied from 0.25 to 3.54 µM. For *Ta*LOX, even though the resulting spectrum takes around 12 times longer to run than *Mo*LOX (**Figure 3.8**), there is a slight linear portion before the final plateau; however, the rate translates to very slow k_{cat} value of ≤ 0.04 s^{-1}, compared to WT *Mo*LOX, k_{cat} of 2.4 s^{-1} (**Table 3.3**). *Pm*LOX did not run to completion. The reaction was allowed to run for up to an hour for the chance to run to completion, but a plateau was never observed. A rate could not be detected from this enzyme, and the reaction resembled the blank reaction. The same could be said of *Cj*LOX (**Figure 3.8**) and the *Mo*LOX leucine clamp to cysteine mutation (L331C) (**Table 3.3**). The slight promise shown by *Ta*LOX lead to future studies being centered around the one class II fungal LOX.

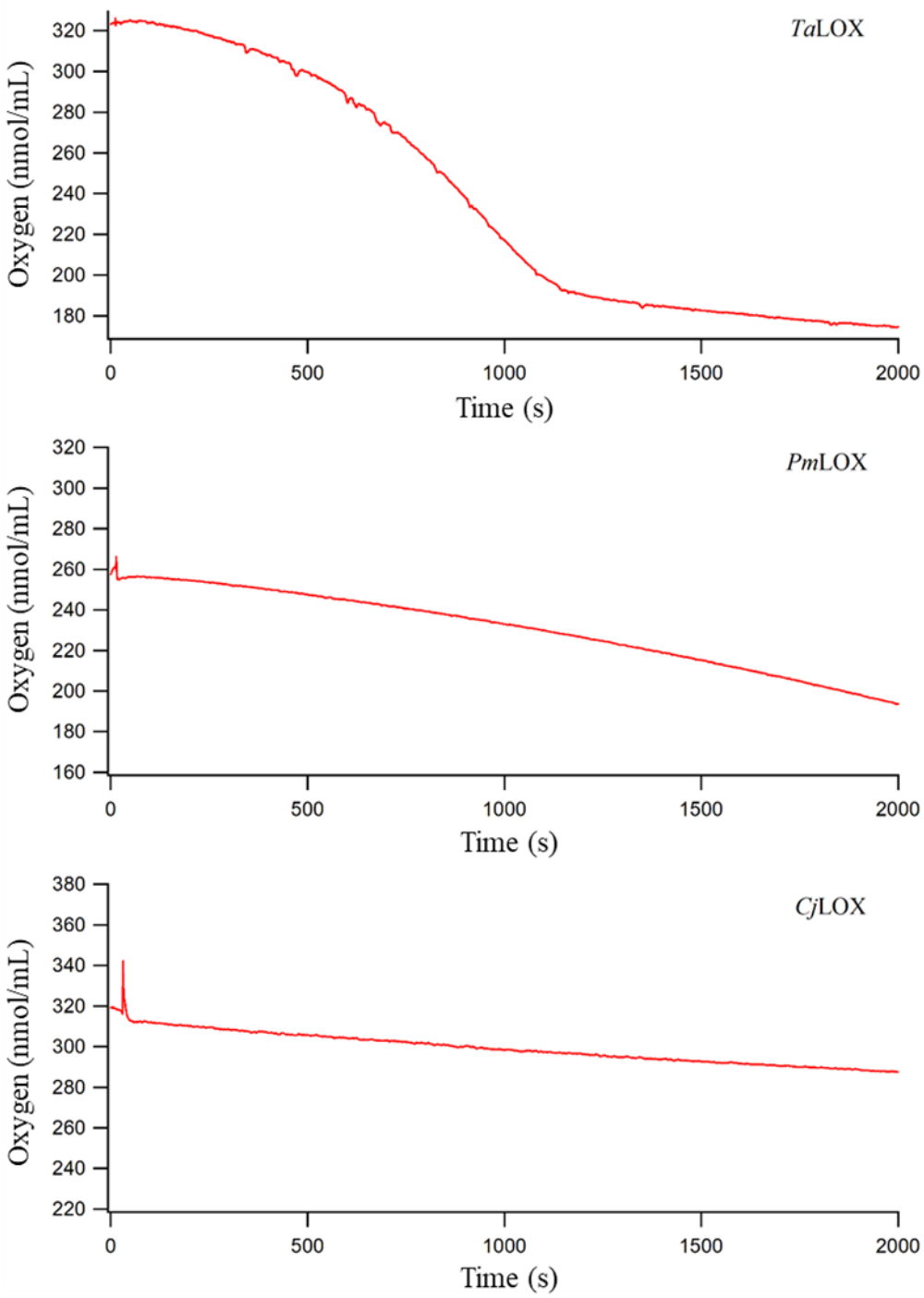

Figure 3.8: *Raw data traces of an oxygen electrode reaction for TaLOX (3.24 µM), PmLOX (3.52 µM), and CjLOX (2.4 µM) measured at 25 °C.*

Table 3.3: *Rate of catalysis of fungal lipoxygenases via O_2 electrode. N.D. is a value not detected by the electrode, suggesting no activity.*

Fungal LOX	k_{cat} **(s^{-1})**
WT-*Mo*LOX	2.4 ± 0.1
*Ta*LOX	≤ 0.048
*Pm*LOX	N.D.
*Cj*LOX	N.D.
*Mo*LOX L331C	N.D.

N.D., not detectable activity. MoLOX is represented as a mean value with ± standard error of the mean from three experiments.

3.5 Metal Analysis of Class II LOXs

Inductively coupled plasma-optical emission spectroscopy (ICP-OES) was used to analyze the metal present in a sample. Plant and animal LOXs contain a non-heme, mononuclear iron center whereas *Mo*LOX and other 'class I' fungal LOXs contain a manganese ion. SLO and *Mo*LOX were used as references, with SLO being the Fe-LOX and *Mo*LOX being the Mn-LOX.[16,42] The ICP-OES data were consistent with these expectations, as SLO had 0.69 Fe atoms per SLO protein and 0.44 Mn atoms per *Mo*LOX protein. ICP-OES of *Ta*LOX and *Pm*LOX samples showed equal parts copper and manganese (**Table 3.4**).

Table 3.4: *Inductively coupled plasma-optical emission spectroscopy metal analysis of SLO, MoLOX and two class II LOXs.*

Enzyme	Copper	Iron	Manganese
SLO	0.04	0.69	0.15
*Mo*LOX	0.13	0.02	0.44
*Ta*LOX	0.31	0.01	0.35
*Pm*LOX	0.31	0.01	0.3

3.6 Steady State Kinetics of SLO "Clamp" Mutations

To determine the functional effect of cysteine at the Leu clamp position, I chose to prepare variants of SLO, a prototype plant LOX. The leucine clamp (L546) of SLO was mutated to a cysteine to mimic the class II fungal LOXs. For completeness, L546 was also mutated to a serine to assess the effect of polarity at this residue. The lack of bulk on the side chains is predicted to prevent proper substrate positioning, which has been reported previously when mutating L546 to an alanine.[32] The three protein variants (L546C, L546S, and L546A) demonstrate a drastic decrease in the first-order (k_{cat}) and second-order (k_{cat}/K_M) rate constants, where k_{cat} represents the overall rate of the reaction and k_{cat}/K_M value represents the efficiency of the enzyme reaction, including substrate capture.

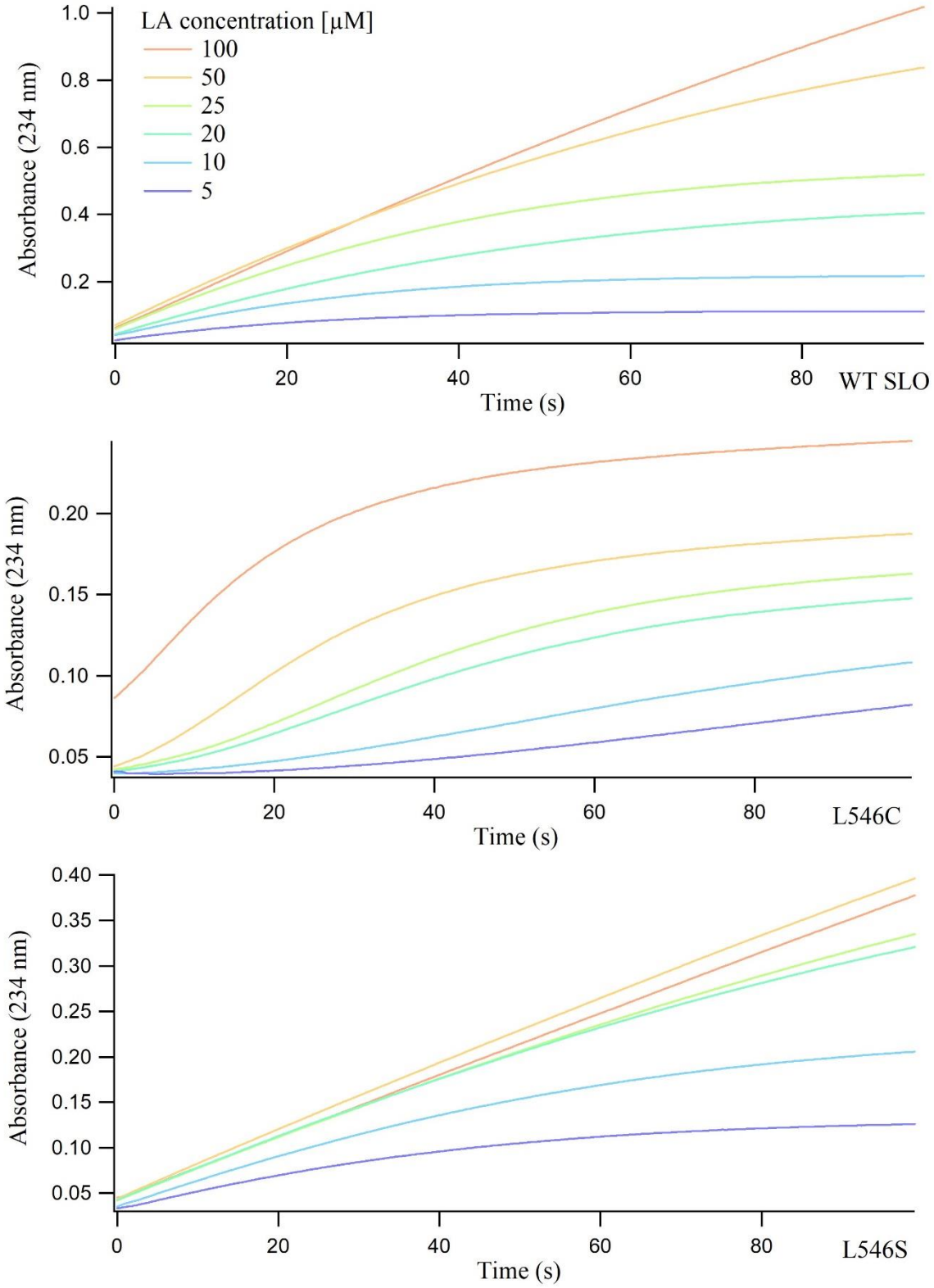

Figure 3.9: *Representative kinetic traces of complete data sets of raw UV-vis traces of reactions at 30 C WT SLO (3.9 nM, top), SLO L546C (70.5 nM, middle), and SLO L546S (42.0 nM, bottom).*

The raw data of L546C and L546S generate different UV-vis kinetic plots. L546C most notably has a lag phase before the reaction proceeds. The three SLO mutations generate similar k_{cat} values, but L546C has a notably lower k_{cat}/K_M value than L546A/S (**Table 3.5**). These data suggest that substrate capture may be less effective than the other SLO variants. In addition, the L546C shows early abortion of turnover, possibly indicating an inhibition effect with product formation. This is not noticeable in other protein variants including L546S.

Table 3.5: *Kinetic analysis of SLO and subsequent mutations used to mimic class II fungal LOXs and the cysteine clamp. The data includes rate of catalysis, k_{cat}/K_M, and KIEs.* [a.] *L546A data was previously measured.*[32]

SLO	k_{cat} (s^{-1})	k_{cat}/K_M (s^{-1} μM^{-1})	KIE
WT	288 (23)	10.7 (2.2)	64 (6)
L546A[a.]	4.8 (0.6)	0.33 (0.1)	93 (9)
L546C	5.2 (0.6)	0.06 (0.01)	75 (15)
L546S	3.9 (0.1)	0.64 (0.09)	109(6)

3.7 Isolation of TaLOX from E. coli cultures

*Ta*LOX was also expressed in and isolated from *E. coli* cultures, to see if the protein might incorporate iron for activity instead of manganese. For example, the fungal LOX *Fusarium graminearum* has been shown to bind iron and has been successfully isolated from *E. coli* cultures.[17]

Samples of the purification were collected after each stage of purification to be analyzed on an SDS-PAGE gel. As seen in **Figure 3.10**, a prominent band in the elution (Buffer B), which migrates approximately at 70 kD, consistent with the predicted weight of *Ta*LOX (**Table 3.2**). The overall conclusion of the expression and purification of TaLOX in *E. coli* is a successfully expressed and isolated target protein.

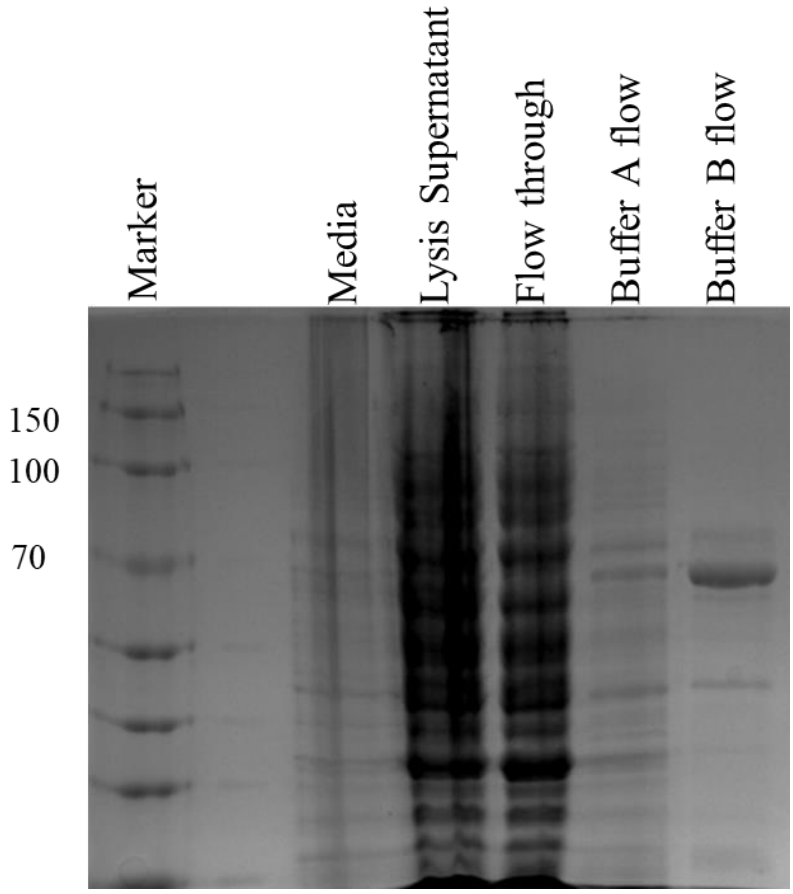

Figure 3.10: *SDS-PAGE analysis of TaLOX expressed in E. coli purification.*

The *Ta*LOX expressed in *E. coli* was also kinetically analyzed using the O_2 electrode. The outcome was still effectively zero (**Figure 3.11**).

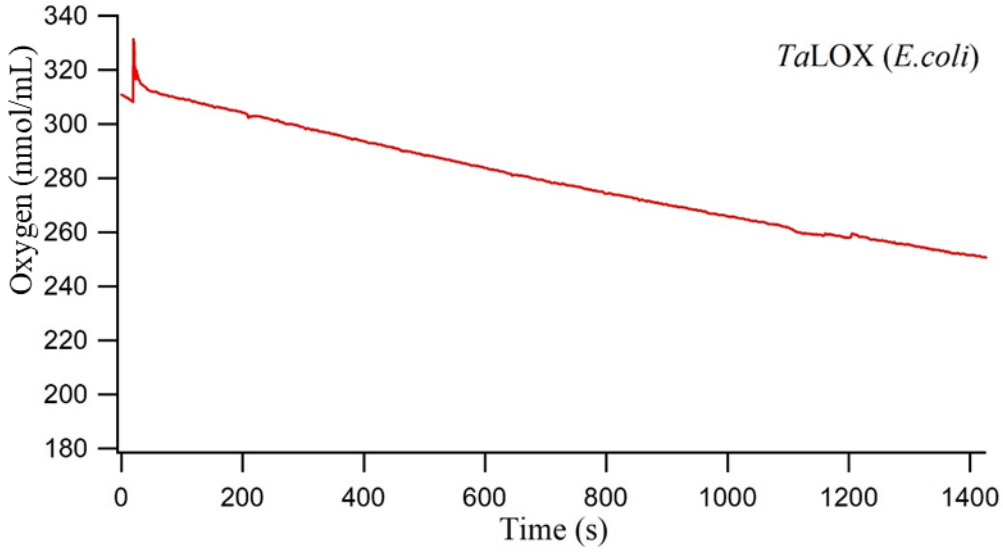

Figure 3.11: *Oxygraph trace of TaLOX isolated from E. coli. 3.24 µM enzyme concentration, 25 °C, 100 µM LA concentration.*

3.8 Ferrozine Assay for iron content analysis

Previously, ICP-OES showed *Ta*LOX did not have a binding preference when expressed in the yeast system, with nearly equivalent Cu and Mn loaded onto the enzyme. To test if Fe could be loaded into *Ta*LOX using *E. coli*, a ferrozine assay was employed. A ferrozine assay is a simple way to test the presence of iron in a sample that could provide insight on protein metal binding in the presence of iron. This assay uses an iron-binding chelator that exhibits a unique absorbance spectrum when iron is bound.

Table 3.6: *Ferrozine assay for iron content in various LOXs. The iron content is a ratio of iron: enzyme in the sample. The higher the content, the more iron per enzyme present in the sample.*

LOX Sample	Fe Content
SLO	0.84
*Ta*LOX *(P.p.*)	0.13
*Ta*LOX (*E.c.*)	0.56
SLO 546S	0.89
SLO 546C	0.80

SLO is used as a reference in this study. SLO expressed in and isolated from *E. coli* showed iron content of approximately 0.8, which is close to the ICP-OES results described above, thus giving confidence in the methods for determining metal content (**Table 3.6**). The SLO variants, L546S and L546C, also bind iron, with ratios of 0.89 and 0.80, respectfully. These values indicate that the catalytic impairment of the mutations does not arise from the lack of metal bound. In comparison, *Ta*LOX expressed in yeast had an iron content of 0.13 Fe atoms per protein, which is consistent with the ICP-OES results that the protein is primarily a Mn binding protein. The *Ta*LOX protein expressed in *E. coli*, however, had an output of 0.56 iron atoms per enzyme.

3.9 Structure prediction of class II fungal LOXs using AlphaFold 3

To obtain structural information on the class II fungal LOXs, AF3 was used to predict protein structures. With an RMSD 0.271 Å, the X-ray crystal structure of *Mo*LOX (PDB: 5FNO)

and the AI generated *Mo*LOX structure align well. Thus, this gives us confidence that AF3 can be used to obtain meaningful structural information on LOX proteins.

*Ta*LOX and *Pm*LOX sequences were inserted to the server for analysis with and without the Fe^{3+}/Mn^{2+} ions to test folding in multiple settings. The folding and confidence of the enzyme models remained consistent with either metal or without. In PyMOL, the RSMD of a *Ta*LOX overlay without and with manganese was 0.174 Å. A low RSMD score and confidence intervals in the high 90's suggest that AF3 does not generate significantly different *Ta*LOX structures in the presence of metal.

The structures of the class II fungal LOXs align similarly to *Mo*LOX in multiple facets (**Figure 3.12**). To summarize, the AF3 structures of class II fungal LOXs i) are predominantly α-helical, ii) have structures of α-helix 2, the C-terminus, and the N-terminus with relating features to prototype fungal LOXs, iii) have predicted primary coordination spheres containing fungal LOX conserved ligands (**Figure 3.13**).

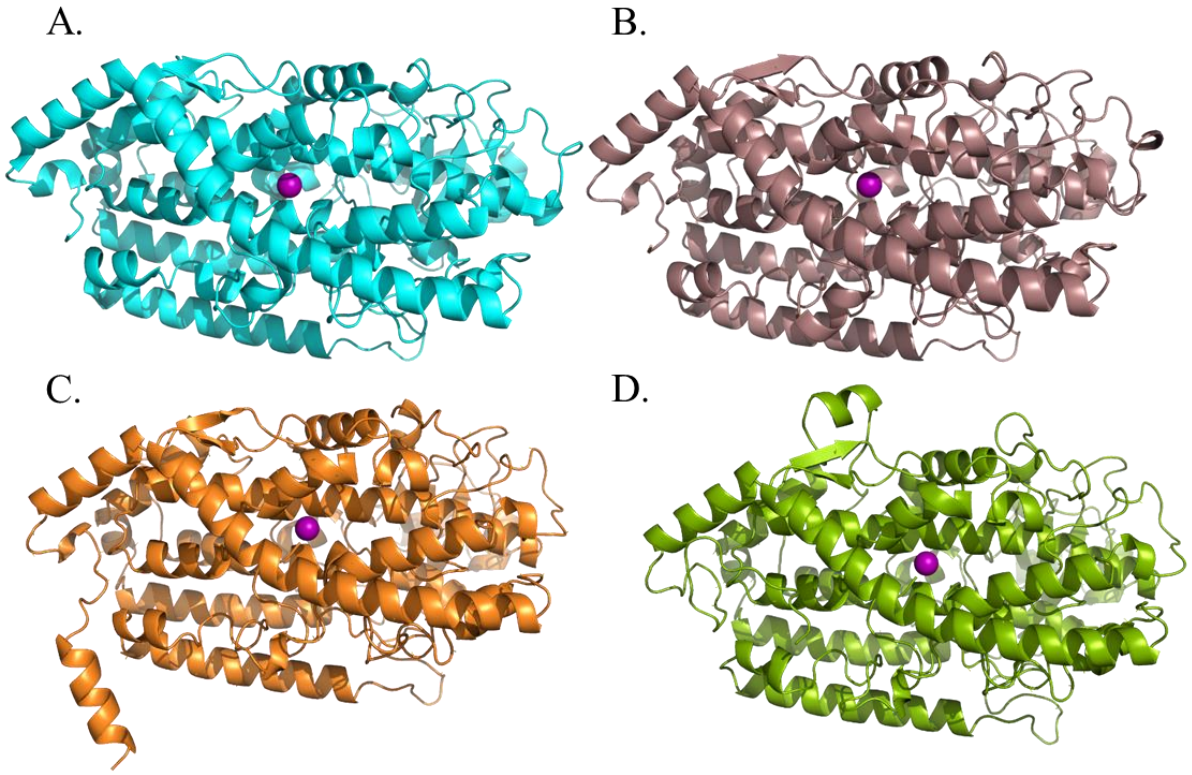

Figure 3.12: *PyMOL structures of the A.) crystal structure of MoLOX and the three AlphaFold 3 generated structures of B.) MoLOX, C.) TaLOX, D.) PmLOX.*

In an overlay of the active sites of the crystal structure of *Mo*LOX and AlphaFold 3 *Mo*LOX, the orientations of the active site residues are nearly identical (**Figure 3.13, left**). The largest difference is apparent in the C-terminal tail of valine, but the carboxyl group is still directed towards the metal in the same facet. The C-terminal tail of valine stands out again, but another difference appears in the prediction of the orientation of His284 in the class II fungal LOXs (**Figure 3.13, right**). Here, the histidine is positioned closer to the metal cofactor than either *Mo*LOX structure.

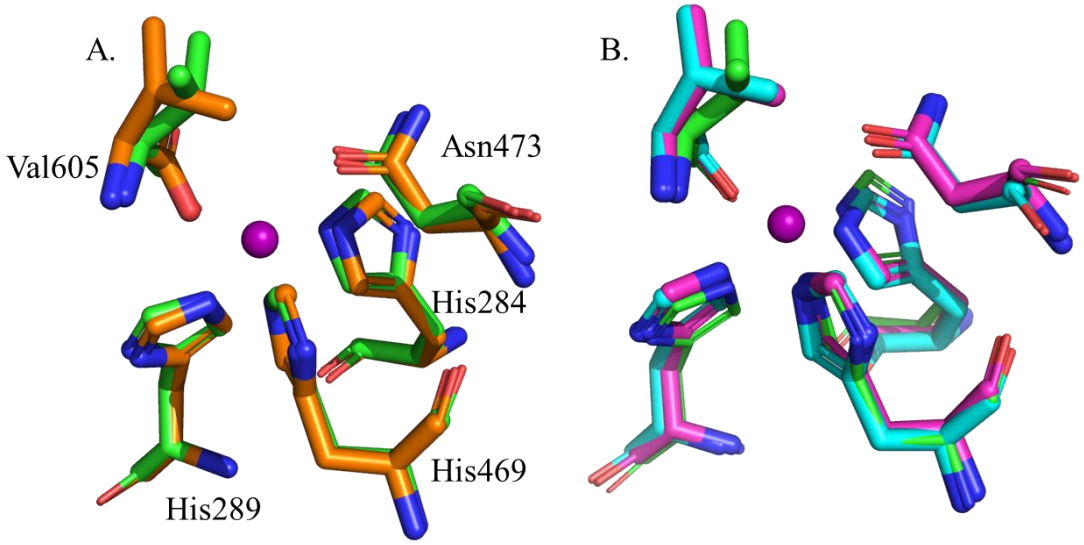

Figure 3.13: *Overlay of active site residues in A. the crystal structure of MoLOX (orange) and the Alphafold 3 generated structure of MoLOX (green), and B.) the Alphafold 3 generated structure of MoLOX, TaLOX (blue), and PmLOX (magenta).*

3.10 Protein folding analysis via circular dichroism spectroscopy (CD)

CD spectroscopy is used to analyze protein folding and secondary structures of the proteins. Proteins that are α-helical will have two minimum peaks at ~222 and 208 nm and a positive band at 193 nm; and proteins that consists predominantly of β-sheets will have a negative peak at 218 nm and a positive peak at 195 nm. SLO consists of a β-sheet PLAT domain and an α-helical catalytic domain. The subsequent CD spectra is consistent with primarily a helical structure. *Mo*LOX is also an enzyme that is structurally predominantly α-helical, being a LOX with a crystal structure lacking the PLAT domain (**Figure 3.14A**).[7,12] These two enzymes can be used as comparisons for the potential class II fungal LOXs. The CD data sets were converted to molar ellipticity to normalize the ellipticity to pathlength and concentration, since the concentrations of the enzymes differed slightly. The protein concentrations were recorded ahead of time for this conversion.

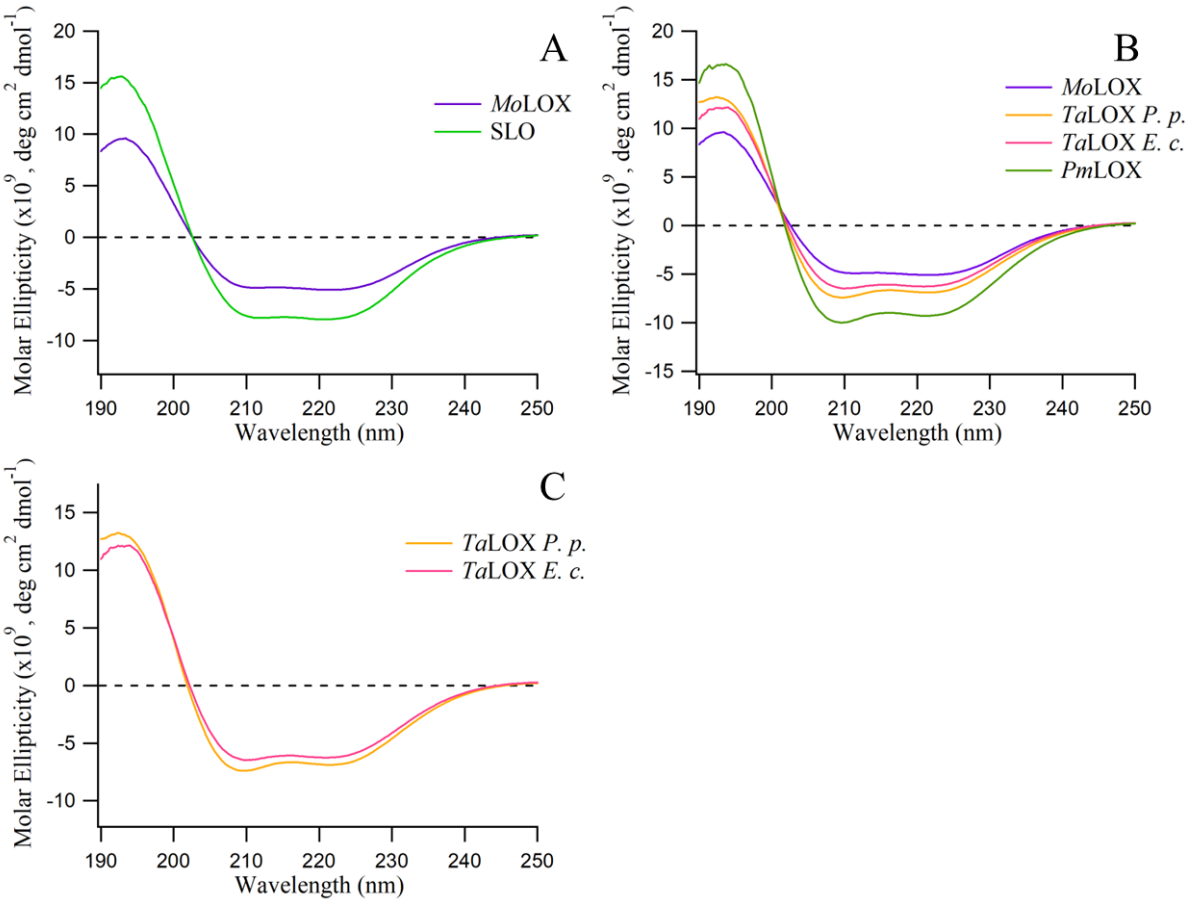

Figure 3.14: *Circular dichroism spectra overlay of A.) MoLOX and SLO, B.) MoLOX, TaLOX in both systems, and PmLOX, C.) TaLOX in P. pastoris and E. coli.*

*Ta*LOX, in *P. pastoris* and *E. coli*, and *Pm*LOX were the two class II LOXs analyzed by circular dichroism. The outcomes are essentially as expected when using the AlphaFold 3 generated structures as a reference (**Figure 3.12**). The three proteins produced spectra of α-helical secondary structures (**Figure 3.14B**). Two things interesting of note are the strong signal from the *Pm*LOX in comparison to *Mo*LOX and *Ta*LOX, and the consistent folding of *Ta*LOX between the two expression systems (**Figure 3.14C**). The reason for a stronger CD spectrum from *Pm*LOX could be from many factors ranging from α-helix count to rigidity.

*Ta*LOX has been successfully expressed in both *P. pastoris* and *E. coli* based on molecular weight only. Here, the protein folding between the two systems can be analyzed and compared. The systems have undergone metal analysis via ICP-OES and the ferrozine assay, kinetic analysis for rate of catalysis, and AI folding analysis through AF3. The two systems thus far reveal many similarities in lacking metal binding preference, essentially no rate detected on the O_2 electrode, and identical folding whether feeding the system iron or manganese through the AI server. Here, there is no difference between them again. *Ta*LOX yields the same CD spectrum regardless of the expression system.

3.11 Differential Scanning Calorimetry (DSC)

Protein folding stability can be measured using DSC. The denaturation of an enzyme is an endothermic reaction because the enthalpy of denaturation is a positive value, meaning energy is absorbed when the protein shifts from folded to denatured. The absorption of energy happens because of overcoming intramolecular hydrogen bonds and electrostatics. The stability of the class II fungal LOX enzymes is analyzed to compare them to the prototype *Mo*LOX. Overall, the melting temperatures (T_M values) and enthalpy of unfolding (ΔH) were fairly similar to that of *Mo*LOX. Coupled with the CD data, these DSC results support that the class II LOXs are well folded.

Furthermore, the SLO mutations, L546C and L546S, can be compared to wildtype SLO to determine the thermodynamic effect of substrate “clamp” mutations. The data are similar, but most notably, SLO L546C has a slightly increased ΔH and T_M value in comparison. The mutated

enzyme with the cysteine in the clamp location may result in a potentially more stable protein, albeit with poor activity compared to WT.

Table 3.7: *DSC data of MoLOX, SLO, class II fungal LOX samples, and SLO class II fungal LOX mimics*

	ΔH (kJ/mol)	**T_M (°C)**
*Mo*LOX	850	63.7
*Ta*LOX *Pp*	1170	59.6
*Ta*LOX *Ec*	615	56.7
*Pm*LOX	1170	59.9
SLO	1552.9	62.7
L546C	1743.2	64.4
L546S	1358.7	62.9

Chapter Four

Discussion

4.1 Presumed Class II fungal LOX Enzymes

The bioinformatics analysis of 48 putative fungal lipoxygenases suggested that there were nine LOXs in a subclass II of fungal lipoxygenases.[20] The main structural property that sets them aside from the prototype 'class I' fungal LOXs is a non-conservative cysteine mutation located at the otherwise conserved leucine clamp residue. The Leu clamp is considered to position substrates with respect to the metal cofactor, allowing wave function overlap for the oxidation of fatty acid substrates to occur. The bulk of this residue is essential to maintain activity, as mutations to volume-reducing side chains, such as alanine, have been previously correlated with decreased activity.[32,43] In this thesis, three representative of the 'class II' fungal LOXs (*Cj*LOX, *Pm*LOX, and *Ta*LOX) were selected for recombinant expression and biochemical characterization.

AF3 models of these three class II fungal LOXs provided confidence that the chosen enzymes fold similarly to *Mo*LOX – a paradigm of the class I pathogenic fungal LOXs. The RSMD values were well within the 2 Å reference point for well aligned structures, and the confidence intervals provided by the server were 90^{+}% confident. The structural models of class II representatives exhibited a helical domain that matched the general structure of a fungal LOX catalytic domain, and α helix-2 found in LOXs used for stability and potentially substrate interactions.[2,7,28] Looking further within, the primary metal-ligand residues of the class II LOXs, including the C-terminal tail, were conserved with similar predicted orientations of the amino

acid sidechains. The metal analysis of *Ta*LOX (isolated from yeast) and *Pm*LOX showed a distribution of manganese and copper binding, whereas the TaLOX protein isolated from bacterial culture had mostly iron bound. This data leads to a lack of clarity in terms of metal binding. It's important to note that AF3 is not well suited to accurately predict whether a metalloenzyme would bind manganese over iron and vice versa.

4.2 Focusing on TaLOX

To maximize efficiency, one of the class II fungal LOXs – *Ta*LOX - was chosen as a focus for further comparative biochemical studies. Knowing that *Ta*LOX nor *Pm*LOX exhibited glycosylation based on SDS-PAGE analysis, and *Ta*LOX showed some, albeit low, kinetic activity, *Ta*LOX was the chosen enzyme. It was the predominant enzyme used for pH preference and substrate specificity studies. It was discovered that the enzyme was poorly active ($k_{cat} < 0.05$ s^{-1}) when LA and αLA were used as a substrate at pH 9.0, but the oxygraphs of the substrate AA and reactions at pH 7.0 are noisy with no obvious oxidation. Initially, the thought was the cysteine clamp was the only factor in the lack of catalysis, but the metal binding was also in question. ICP-OES revealed equal amounts of copper and manganese within the *Ta*LOX and *Pm*LOX samples with essentially trace amounts of iron. Previous variants of *Mo*LOX with high contaminating Cu concentrations are inactive and select fungal LOXs have been isolated as functional iron-containing enzymes.[17,43] Yeast is not well suited for loading iron, so expressing in a different system could lead to iron loading and an active enzyme. *F. graminearus* is a fungal LOX that had previously been expressed and purified in *E. coli* and bound iron, so the next step in the process of characterizing these class II LOXs was to express *Ta*LOX in *E. coli* and test iron content and kinetic activity.[17] The ferrozine assay of *Ta*LOX isolated from *E. coli* cultures resulted in 56% iron content, which is much lower than the Fe-LOX of SLO. This is not a

promising result because it indicates that only half of the enzyme present in the sample contained iron, suggesting that the enzyme only weakly coordinated the enzyme. The enzymes expressed in yeast and in *E. coli* migrated to the predicted weight and produced similar CD spectra when analyzed. Despite this, the activity of this *Ta*LOX protein was nearly zero. Thus, the lack of activity of *Ta*LOX was not assumed to be attributed to a specific metal or unfolded protein.

4.3 SLO Mimic Mutational Study

The plant LOX, SLO, has been used extensively for structure-function studies.[44] It is a stable system that has often been the focus of LOX mutational studies, since LOXs have many conserved residues.[27,45,46] SLO exhibits fast LOX activity and the initial PCET step is rate-determining, as shown by its large KIE for the oxidation of linoleic acid. In this thesis, the leucine clamp of SLO, L546, was mutated to Cys to examine (and mimic) the functional and structural consequences of the non-conservative mutation of class II fungal LOXs.

The conserved leucine clamp of lipoxygenases does not directly ligate the metal cluster, so it is not regarded as being involved in metal loading. Herein, that result is consistent. The ferrozine assay, which entails a spectroscopic approach to quantify the concentration of iron using a ferrous iron chelator, showed that the SLO mimics generally have comparable iron content (0.8 iron atoms per protein). Furthermore, DSC studies show that the Leu-to-Cys mutation does not affect protein folding or stability, with the variants displaying relatively alike enthalpies of unfolding and melting temperatures.

The major difference between wildtype SLO and the two mutations in this study resides in the activity of the enzyme. Perhaps the most telling results of the entire study involve the kinetic activity of the SLO enzyme variants, specifically with L546C. In addition to the reduced

k_{cat}, the reaction of L546C with LA contains a lag phase, meaning product formation is delayed. This could be attributed to either a sluggish binding of substrate and/or a slowed activation of the enzyme. For the latter, LOXs are isolated with the metal in the 2+ oxidation state that gets converted to the 3+ oxidation state upon aerobic incubation of the enzyme with substrate. Consistent with the former, the K_M value (half V_{max}) of the L546C enzyme variant is much higher in comparison to WT SLO and other SLO clamp mutations (e.g., L546A/S). An elevated K_M value can be indicative of weak binding of substrate (low substrate affinity) as the enzyme requires a higher concentration of substrate to reach half V_{max}. The K_M of the L546C variant was three-fold higher compared to wildtype SLO even with a much slower k_{cat}. This could be from interactions between the substrate and enzyme outside of the metal alone, and the only difference in the two enzymes is the mutated Leu-to-Cys clamp. The cysteine clamp could prevent proper substrate positioning leading to both a lack of substrate binding and even inhibit product formation.

In addition to the observation of a lag phase for initiation of substrate oxidation, the reaction of the L546C exhibits early abortion. At the highest LA concentration, L546C shows only 20% of the total product turnover compared to that of WT or L546S. This effect could stem from the formation of the hydroperoxide product binding tightly to the enzyme complex, thus leading to inhibition of the enzyme. Since the K_M is higher for substrate to L546C compared to the other variants, this is unlikely. Alternatively, the formed hydroperoxide could potentially react with the Cys sidechain, thus trapping the product on the enzyme. Cysteine is a redox-active amino acid that undergoes oxidation in cells as part of signaling pathways. Future mass spectrometry studies are required to validate this hypothesis.

Previous SLO kinetic studies can help to explain the functional significance of the enlarged KIE values. The SLO L546A clamp variant was previously shown to increase the KIE from ~60 to 90.[47] This could suggest a potential impact on the tunneling properties at the active site. A more sensitive kinetic property, which can be used to characterize the efficiency of hydrogen tunneling in these enzymes, is the magnitude of the temperature dependence of the KIEs, i.e. ΔE_a. This kinetic feature compares the activation energy (E_a) of the enzyme in the presence of natural substrate versus the deuterated substrate ($\Delta E_a = E_a(D) - E_a(H)$).[10] Deuterium is a heavy isotope of the hydrogen atom, so the energy necessary to overcome the energy barrier is increased; furthermore, the zero point energy (ZPE) of deuterium is lower than that of hydrogen because of the increase in weight, thus leading to a decrease in the length of the wavefunction. If the enzyme is tunneling efficiently, such as the case in wild-type enzymes, the ΔE_a values will be close to zero, because the wavefunctions between donor and acceptor pairs overlap efficiently. What is seen in the case of SLO and the L546A clamp mutation is both an increase in KIEs and ΔE_a, with the latter increasing from 0.9 kcal/mol (WT) to 2 kcal/mol in the

variant.[47] This indicates the tunneling mechanism of the variant decreases in efficiency. The reason for this involved the lack of the bulk residue found in the substrate binding pocket. SLO has a rigid binding pocket to generate an appropriate donor acceptor distance (DAD) for wave function overlap to promote effective tunneling. When this bulky residue is removed, the binding pocket can relax, and the DAD increases, which hinders wave function overlap and decreases the efficiency of proton transfer (hence an increase in the KIE and ΔE_a).

The KIE of the L546S variant is elevated with respect to WT and consistent with L546A. The L546C variant, however, has a large uncertainty in the KIE, so it is difficult to assess the kinetic impact. These enlarged KIE values can serve as a proxy for ΔE_a based on previous kinetic trends observed for L546A. The large, branched Leu residue was mutated to smaller residues that are also polar. It can be assumed that the DAD in these enzymes has increased, which alone decreases the tunneling probability and thus leads to an observed decrease in k_{cat}. For L546C, obtaining the ΔE_a would be difficult, as the large K_M values would provide unreliable k_{cat} values across the temperature range needed to calculate activation energies.

4.4 Concluding Remarks

Other than sharing some structural similarities to fungal LOXs, the collective biochemical data presented in this Thesis suggests that these predicted class II fungal LOXs are not effective as such. This is further suggested by the poor and abortive enzymatic activity of the L546C SLO variant. The purpose of these class II fungal LOX enzymes being encoded in the genome of these organisms remains unknown. They could have been useful previously and have become an evolutionary relic, like human vestigial organs. These enzymes are predicted to be

secreted, but overtime a change in host preference might have led to a decrease in need.[20] Alternatively, they may play a role in fatty acid transport or fatty acid-dependent oxidative stress by binding oxidized lipid products.

4.5 Future Directions

The use of *in vitro* studies on these potential fungal LOXs has not proved to be effective in elucidating the function of these enzymes. Fungal LOXs, such as GgLOX, are initially isolated from their host organism and characterized.[15] The next steps for studies involving the class II fungal LOXs should begin by attempting to isolate the enzyme from the host organism. Also, a metabolomics study of these class II fungal LOXs could prove effective. The host organism could be grown up as a "knock-out" variant without the LOX gene, and then be introduced to their target organism. The pathogenesis of the knock-out organism would provide details on the importance of the LOX gene to the enzyme.

References

(1) Brash, A. R. Lipoxygenases: Occurrence, Functions, Catalysis, and Acquisition of Substrate. *Journal of Biological Chemistry* **1999**, *274* (34), 23679–23682. https://doi.org/10.1074/jbc.274.34.23679.

(2) Offenbacher, A. R.; Holman, T. R. Fatty Acid Allosteric Regulation of C-H Activation in Plant and Animal Lipoxygenases. *Molecules* **2020**, *25* (15), 3374. https://doi.org/10.3390/molecules25153374.

(3) Oliw, E. H. Iron and Manganese Lipoxygenases of Plant Pathogenic Fungi and Their Role in Biosynthesis of Jasmonates. *Archives of Biochemistry and Biophysics* **2022**, *722*, 109169. https://doi.org/10.1016/j.abb.2022.109169.

(4) Hamberg, M.; Gardner, H. W. Oxylipin Pathway to Jasmonates: Biochemistry and Biological Significance. *Biochimica et Biophysica Acta (BBA) - Lipids and Lipid Metabolism* **1992**, *1165* (1), 1–18. https://doi.org/10.1016/0005-2760(92)90069-8.

(5) Henderson, W. R. The Role of Leukotrienes in Inflammation. *Ann Intern Med* **1994**, *121* (9), 684–697. https://doi.org/10.7326/0003-4819-121-9-199411010-00010.

(6) Skrzypczak-Jankun, E.; Funk, M. O. Lipoxygenase: A Molecular Complex with a Non-Heme Iron. **1996**.

(7) Wennman, A.; Oliw, E. H.; Karkehabadi, S.; Chen, Y. Crystal Structure of Manganese Lipoxygenase of the Rice Blast Fungus Magnaporthe Oryzae. *Journal of Biological Chemistry* **2016**, *291* (15), 8130–8139. https://doi.org/10.1074/jbc.M115.707380.

(8) Whittington, C.; Sharma, A.; Hill, S. G.; Iavarone, A. T.; Hoffman, B. M.; Offenbacher, A. R. Impact of N-Glycosylation on Protein Structure and Dynamics Linked to Enzymatic C–

H Activation in the M. Oryzae Lipoxygenase. *Biochemistry* **2024**. https://doi.org/10.1021/acs.biochem.4c00109.

(9) Offenbacher, A. R.; Hu, S.; Poss, E. M.; Carr, C. A. M.; Scouras, A. D.; Prigozhin, D. M.; Iavarone, A. T.; Palla, A.; Alber, T.; Fraser, J. S.; Klinman, J. P. Hydrogen–Deuterium Exchange of Lipoxygenase Uncovers a Relationship between Distal, Solvent Exposed Protein Motions and the Thermal Activation Barrier for Catalytic Proton-Coupled Electron Tunneling. *ACS Cent. Sci.* **2017**, *3* (6), 570–579. https://doi.org/10.1021/acscentsci.7b00142.

(10) Klinman, J. P.; Offenbacher, A. R. Understanding Biological Hydrogen Transfer Through the Lens of Temperature Dependent Kinetic Isotope Effects. *Acc. Chem. Res.* **2018**, *51* (9), 1966–1974. https://doi.org/10.1021/acs.accounts.8b00226.

(11) Newcomer, M. E.; Brash, A. R. The Structural Basis for Specificity in Lipoxygenase Catalysis. *Protein Science* **2015**, *24* (3), 298–309. https://doi.org/10.1002/pro.2626.

(12) Minor, W.; Steczko, J.; Stec, B.; Otwinowski, Z.; Bolin, J. T.; Walter, R.; Axelrod, B. Crystal Structure of Soybean Lipoxygenase L-1 at 1.4 Å Resolution,. *Biochemistry* **1996**, *35* (33), 10687–10701. https://doi.org/10.1021/bi960576u.

(13) Rohlik, D. L.; Patel, E.; Gilbert, N. C.; Offenbacher, A. R.; Garcia, B. L. Investigating Membrane-Binding Properties of Lipoxygenases Using Surface Plasmon Resonance. *Biochemical and Biophysical Research Communications* **2023**, *670*, 47–54. https://doi.org/10.1016/j.bbrc.2023.05.066.

(14) Su, C.; Oliw, E. H. Manganese Lipoxygenase. *Journal of Biological Chemistry* **1998**, *273* (21), 13072–13079. https://doi.org/10.1074/jbc.273.21.13072.

(15) Su, C.; Oliw, E. H. Manganese Lipoxygenase: PURIFICATION AND CHARACTERIZATION *. *Journal of Biological Chemistry* **1998**, *273* (21), 13072–13079. https://doi.org/10.1074/jbc.273.21.13072.

(16) Wennman, A.; Jernerén, F.; Magnuson, A.; Oliw, E. H. Expression and Characterization of Manganese Lipoxygenase of the Rice Blast Fungus Reveals Prominent Sequential Lipoxygenation of α-Linolenic Acid. *Archives of Biochemistry and Biophysics* **2015**, *583*, 87–95. https://doi.org/10.1016/j.abb.2015.07.014.

(17) Brodhun, F.; Cristobal-Sarramian, A.; Zabel, S.; Newie, J.; Hamberg, M.; Feussner, I. An Iron 13S-Lipoxygenase with an α-Linolenic Acid Specific Hydroperoxidase Activity from Fusarium Oxysporum. *PLOS ONE* **2013**, *8* (5), e64919. https://doi.org/10.1371/journal.pone.0064919.

(18) Wennman, A.; Oliw, E. H. Secretion of Two Novel Enzymes, Manganese 9S-Lipoxygenase and Epoxy Alcohol Synthase, by the Rice Pathogen Magnaporthe Salvinii. *Journal of Lipid Research* **2013**, *54* (3), 762–775. https://doi.org/10.1194/jlr.M033787.

(19) Offenbacher, A. R.; Iavarone, A. T.; Klinman, J. P. Hydrogen–Deuterium Exchange Reveals Long-Range Dynamical Allostery in Soybean Lipoxygenase. *J Biol Chem* **2018**, *293* (4), 1138–1148. https://doi.org/10.1074/jbc.M117.817197.

(20) Oliw, E. H. Diversity of the Manganese Lipoxygenase Gene Family – A Mini-Review. *Fungal Genetics and Biology* **2022**, *163*, 103746. https://doi.org/10.1016/j.fgb.2022.103746.

(21) Sugio, A.; Østergaard, L. H.; Matsui, K.; Takagi, S. Characterization of Two Fungal Lipoxygenases Expressed in *Aspergillus Oryzae*. *Journal of Bioscience and Bioengineering* **2018**, *126* (4), 436–444. https://doi.org/10.1016/j.jbiosc.2018.04.005.

(22) Dean, R.; Van Kan, J. a. L.; Pretorius, Z. A.; Hammond-Kosack, K. E.; Di Pietro, A.; Spanu, P. D.; Rudd, J. J.; Dickman, M.; Kahmann, R.; Ellis, J.; Foster, G. D. The Top 10 Fungal Pathogens in Molecular Plant Pathology. *Molecular Plant Pathology* **2012**, *13* (4), 414–430. https://doi.org/10.1111/j.1364-3703.2011.00783.x.

(23) Kostenko, A.; Ray, K.; Iavarone, A. T.; Offenbacher, A. R. Kinetic Characterization of the C–H Activation Step for the Lipoxygenase from the Pathogenic Fungus Magnaporthe Oryzae: Impact of N-Linked Glycosylation. *Biochemistry* **2019**, *58* (29), 3193–3203. https://doi.org/10.1021/acs.biochem.9b00467.

(24) An, H. J.; Gip, P.; Kim, J.; Wu, S.; Park, K. W.; McVaugh, C. T.; Schaffer, D. V.; Bertozzi, C. R.; Lebrilla, C. B. Extensive Determination of Glycan Heterogeneity Reveals an Unusual Abundance of High Mannose Glycans in Enriched Plasma Membranes of Human Embryonic Stem Cells. *Mol Cell Proteomics* **2012**, *11* (4), M111.010660. https://doi.org/10.1074/mcp.M111.010660.

(25) Sharma, A.; Whittington, C.; Jabed, M.; Hill, S. G.; Kostenko, A.; Yu, T.; Li, P.; Hoffman, B. M.; Offenbacher, A. R. 13C ENDOR Spectroscopy-Guided MD Computations Reveals the Structure of the Enzyme-Substrate Complex of an Active, N-Linked Glycosylated Lipoxygenase. bioRxiv December 7, 2022, p 2022.12.07.519351. https://doi.org/10.1101/2022.12.07.519351.

(26) Guevara, L.; Gouge, M.; Ohler, A.; Hill, S. G.; Patel, S.; Offenbacher, A. R. Effect of Solvent Viscosity on the Activation Barrier of Hydrogen Tunneling in the Lipoxygenase Reaction. *Archives of Biochemistry and Biophysics* **2023**, *747*, 109740. https://doi.org/10.1016/j.abb.2023.109740.

(27) Horitani, M.; Offenbacher, A. R.; Carr, C. A. M.; Yu, T.; Hoeke, V.; Cutsail, G. E. I.; Hammes-Schiffer, S.; Klinman, J. P.; Hoffman, B. M. 13C ENDOR Spectroscopy of Lipoxygenase–Substrate Complexes Reveals the Structural Basis for C–H Activation by Tunneling. *J. Am. Chem. Soc.* **2017**, *139* (5), 1984–1997. https://doi.org/10.1021/jacs.6b11856.

(28) Chen, Y.; Wennman, A.; Karkehabadi, S.; Engström, Å.; Oliw, E. H. Crystal Structure of Linoleate 13R-Manganese Lipoxygenase in Complex with an Adhesion Protein1. *Journal of Lipid Research* **2016**, *57* (8), 1574–1588. https://doi.org/10.1194/jlr.M069617.

(29) Nelson, M. J. Catecholate Complexes of Ferric Soybean Lipoxygenase 1. *Biochemistry* **1988**, *27* (12), 4273–4278. https://doi.org/10.1021/bi00412a011.

(30) Ishikita, H.; Loll, B.; Biesiadka, J.; Saenger, W.; Knapp, E.-W. Redox Potentials of Chlorophylls in the Photosystem II Reaction Center. *Biochemistry* **2005**, *44* (10), 4118–4124. https://doi.org/10.1021/bi047922p.

(31) Hu, S.; Offenbacher, A. R.; Lu, E. D.; Klinman, J. P. Comparative Kinetic Isotope Effects on First- and Second-Order Rate Constants of Soybean Lipoxygenase Variants Uncover a Substrate-Binding Network. *Journal of Biological Chemistry* **2019**, *294* (48), 18069–18076. https://doi.org/10.1074/jbc.RA119.010826.

(32) Knapp, M. J.; Rickert, K.; Klinman, J. P. Temperature-Dependent Isotope Effects in Soybean Lipoxygenase-1: Correlating Hydrogen Tunneling with Protein Dynamics. *J. Am. Chem. Soc.* **2002**, *124* (15), 3865–3874. https://doi.org/10.1021/ja012205t.

(33) Paulsen, C. E.; Carroll, K. S. Cysteine-Mediated Redox Signaling: Chemistry, Biology, and Tools for Discovery. *Chem. Rev.* **2013**, *113* (7), 4633–4679. https://doi.org/10.1021/cr300163e.

(34) Harman, G. E.; Howell, C. R.; Viterbo, A.; Chet, I.; Lorito, M. Trichoderma Species — Opportunistic, Avirulent Plant Symbionts. *Nat Rev Microbiol* **2004**, *2* (1), 43–56. https://doi.org/10.1038/nrmicro797.

(35) Yakti, W.; Kovács, G. M.; Vági, P.; Franken, P. Impact of Dark Septate Endophytes on Tomato Growth and Nutrient Uptake. *Plant Ecology & Diversity* **2018**, *11* (5–6), 637–648. https://doi.org/10.1080/17550874.2019.1610912.

(36) Ou, D.; Zhang, L.; Guo, C.; Chen, X.; Ali, S.; Qiu, B. Identification of a New Cordyceps Javanica Fungus Isolate and Its Toxicity Evaluation against Asian Citrus Psyllid. *Microbiologyopen* **2018**, *8* (6), e00760. https://doi.org/10.1002/mbo3.760.

(37) Borngräber, S.; Browner, M.; Gillmor, S.; Gerth, C.; Anton, M.; Fletterick, R.; Kühn, H. Shape and Specificity in Mammalian 15-Lipoxygenase Active Site: THE FUNCTIONAL INTERPLAY OF SEQUENCE DETERMINANTS FOR THE REACTION SPECIFICITY*. *Journal of Biological Chemistry* **1999**, *274* (52), 37345–37350. https://doi.org/10.1074/jbc.274.52.37345.

(38) Jakobowski, A.; Hill, S. G.; Guy, S. W.; Offenbacher, A. R. Substitution of the Mononuclear, Non-Heme Iron Cofactor in Lipoxygenases for Structural Studies. In *Methods in Enzymology*; Academic Press, 2024. https://doi.org/10.1016/bs.mie.2024.05.011.

(39) Abramson, J.; Adler, J.; Dunger, J.; Evans, R.; Green, T.; Pritzel, A.; Ronneberger, O.; Willmore, L.; Ballard, A. J.; Bambrick, J.; Bodenstein, S. W.; Evans, D. A.; Hung, C.-C.; O'Neill, M.; Reiman, D.; Tunyasuvunakool, K.; Wu, Z.; Žemgulytė, A.; Arvaniti, E.; Beattie, C.; Bertolli, O.; Bridgland, A.; Cherepanov, A.; Congreve, M.; Cowen-Rivers, A. I.; Cowie, A.; Figurnov, M.; Fuchs, F. B.; Gladman, H.; Jain, R.; Khan, Y. A.; Low, C. M.

R.; Perlin, K.; Potapenko, A.; Savy, P.; Singh, S.; Stecula, A.; Thillaisundaram, A.; Tong, C.; Yakneen, S.; Zhong, E. D.; Zielinski, M.; Žídek, A.; Bapst, V.; Kohli, P.; Jaderberg, M.; Hassabis, D.; Jumper, J. M. Accurate Structure Prediction of Biomolecular Interactions with AlphaFold 3. *Nature* **2024**, 1–3. https://doi.org/10.1038/s41586-024-07487-w.

(40) Asbi, B. A.; Wei, L. S.; Steinberg, M. P. Effect of pH on the Kinetics of Soybean Lipoxygenase-1. *Journal of Food Science* **1989**, *54* (6), 1594–1595. https://doi.org/10.1111/j.1365-2621.1989.tb05167.x.

(41) Joshi, N.; Hoobler, E. K.; Perry, S.; Diaz, G.; Fox, B.; Holman, T. R. Kinetic and Structural Investigations into the Allosteric and pH Effect on the Substrate Specificity of Human Epithelial 15-Lipoxygenase-2. *Biochemistry* **2013**, *52* (45), 8026–8035. https://doi.org/10.1021/bi4010649.

(42) Pistorius, E. K.; Axelrod, B. Iron, an Essential Component of Lipoxygenase. *Journal of Biological Chemistry* **1974**, *249* (10), 3183–3186. https://doi.org/10.1016/S0021-9258(19)42656-2.

(43) Sharma, A.; Whittington, C.; Jabed, M.; Hill, S. G.; Kostenko, A.; Yu, T.; Li, P.; Doan, P. E.; Hoffman, B. M.; Offenbacher, A. R. 13C Electron Nuclear Double Resonance Spectroscopy-Guided Molecular Dynamics Computations Reveal the Structure of the Enzyme–Substrate Complex of an Active, N-Linked Glycosylated Lipoxygenase. *Biochemistry* **2023**, *62* (10), 1531–1543. https://doi.org/10.1021/acs.biochem.3c00119.

(44) Klinman, J. P.; Kohen, A. Hydrogen Tunneling Links Protein Dynamics to Enzyme Catalysis. *Annual Review of Biochemistry* **2013**, *82* (Volume 82, 2013), 471–496. https://doi.org/10.1146/annurev-biochem-051710-133623.

(45) Hu, S.; Offenbacher, A. R.; Thompson, E. M.; Gee, C. L.; Wilcoxen, J.; Carr, C. A. M.; Prigozhin, D. M.; Yang, V.; Alber, T.; Britt, R. D.; Fraser, J. S.; Klinman, J. P. Biophysical Characterization of a Disabled Double Mutant of Soybean Lipoxygenase: The "Undoing" of Precise Substrate Positioning Relative to Metal Cofactor and an Identified Dynamical Network. *J. Am. Chem. Soc.* **2019**, *141* (4), 1555–1567. https://doi.org/10.1021/jacs.8b10992.

(46) Sharma, S. C.; Klinman, J. P. Kinetic Detection of Orthogonal Protein and Chemical Coordinates in Enzyme Catalysis: Double Mutants of Soybean Lipoxygenase. *Biochemistry* **2015**, *54* (35), 5447–5456. https://doi.org/10.1021/acs.biochem.5b00374.

(47) Knapp, M. J.; Rickert, K.; Klinman, J. P. Temperature-Dependent Isotope Effects in Soybean Lipoxygenase-1: Correlating Hydrogen Tunneling with Protein Dynamics. *J. Am. Chem. Soc.* **2002**, *124* (15), 3865–3874. https://doi.org/10.1021/ja012205t.